Evaluation of substrates for surface-enhanced Raman scattering

by

Muyang Zhong
B.Sc, Beihang University, 2013

A Thesis Submitted in Partial Fulfillment
of the Requirements for the Degree of

MASTER OF SCIENCE

in the Department of Physics

Supervisory Committee

Evaluation of substrates for surface-enhanced Raman scattering

by

Muyang Zhong
B.Sc., Beihang University, 2013

Supervisory Committee

Dr. Alexandre G. Brolo, (Department of Chemistry)
Supervisor

Dr. Byoung-Chul Choi, (Department of Physics)
Departmental Member

Dr. Geoffrey M. Steeves, (Department of Physics)
Departmental Member

Abstract

Supervisory Committee
Dr. Alexandre G. Brolo, (Department of Chemistry)
Supervisor
Dr. Byoung-Chul Choi, (Department of Physics)
Departmental Member
Dr. Geoffrey M. Steeves, (Department of Physics)
Departmental Member

Surface-enhanced Raman scattering (SERS) has long been the interest of researchers in chemistry, physics and engineering, especially since the discovery that SERS can probe into the system down to the single molecule (SM) level. Despite the large number of publications regarding the fabrication of SERS substrates, it has been a challenge in the field to quantify the SERS signal and universally compare substrates. Traditionally, enhancement factor (EF) is used as an indicator of substrate quality, but the EF calculation is hugely dependent on the estimation of the surface coverage and other factors that are determined largely subjectively. Therefore, this thesis aims at discussing other parameters that can also be used to evaluate different substrates.

Six different SERS substrates of Ag or Au nanoparticles of different sizes were fabricated by nanosphere lithography (NSL) and characterized by electron microscopy and UV-vis spectroscopy. SERS substrates were mapped for different concentrations of a probe molecule. Through subsequent baseline correction and principle component analysis (PCA), the "intensity" of individual spectrum was obtained and the shapes of intensity histograms of each substrate were acquired.

Instead of calculating EF, five criteria (six quantification methods in total) were employed to comprehensively evaluate the six substrates. These were density of hot spots (characterized by the number of zero-intensity events), enhancement (represented by mean intensity), spatial variation (calculated by RSD of intensity), repeatability (realized by cross correlation) and histogram shape (quantified by skewness and kurtosis). These new methods provide insights to the understanding

of the properties of SERS substrates in terms of hot spots. Different substrates may exhibit better performance in terms of one criterion but worse in terms of others. Those variations in performance can be explained by their surface morphology.

These more elaborated methods are believed to provide a more comprehensive approach to evaluate and compare substrates than the traditional EF values. The thesis also paves the way for future study on SM-SERS and fabricating better SERS substrates.

Table of Contents

List of Tables

List of Figures

Acknowledgments

I would like to thank Dr. Alexandre Brolo for his support in my scientific journey. He is always helpful and approachable and I cannot finish this program without many intellectually stimulating conversations with him. I am also grateful for the friendly atmosphere of the whole research group and many helpful exchanges from group members. I would also like to thank Alex W. for his generous help with Raman instrumentation and data analysis, Chris in the machine shop for fabricating the SERS cell for me and Elaine for helping me with the operation of SEM.

Dedication

To my family members, friends and myself.

Chapter 1 Background

In this chapter, we present an introduction to the history and basics of Raman scattering, surface-enhanced Raman scattering (SERS), and single-molecule SERS (SM-SERS) to set the current work into a relevant context.

1.1 Raman scattering

Raman scattering is an inelastic scattering that carries information about the energy of the vibrational levels of a molecule. When an incoming photon interacts with a molecule in a material, two types of scattering can happen: i) Rayleigh (elastic) scattering. In this case, the energy of incoming photon remains unchanged after scattering; ii) Stokes or anti-Stokes Raman scattering. In these cases, there is an energy shift, i.e. energy of the scattered photon changes relative to the incident photon due to the inelastic scattering. The second type of scattering, called Raman scattering, was theoretically predicted by Smekal et al.[1] in 1923 and experimentally verified in 1928 by C.V. Raman[2], who used converged natural sunlight as the light source and dust-free liquids or gases as scattering media.

The Raman spectra vary from molecule to molecule in that different functional groups (hence different Raman modes) will yield different Raman peaks. Thus, Raman spectroscopy provides a "fingerprint" for molecular detection, making it possible to study the composition and chemical identification of a compound. However, the intensity of normal Raman scattering is weak due to the low probability for an incoming photon to experience Raman scattering. Therefore, strong illumination is required to obtain descent signals. Additionally, it is hard to detect the signal when the background is contaminated with fluorescence. Light sources for Raman measurements before the 1960s were mainly mercury arc lamps with low intensity, thus making the Raman signal very difficult to detect, limiting the applications of Raman spectroscopy.

The laser source, which is monochromatic, directional, and coherent, has become the ideal light source of Raman spectroscopy. Since then, Raman spectroscopy has found increasing applications in chemistry[3], physics[4], mechanics[5], biology[6], and environmental science[7].

The full detail of the mathematical and physical treatment of Raman scattering can be found in many textbooks[8] and/or similar reviews[9] for interested readers.

1.2 Surface-Enhanced Raman Scattering (SERS)

In 1974 Fleischmann et al.[10] observed the Raman signal from pyridine absorbed on a rough Ag surface and found that the Raman signal intensity was unexpectedly high. Initially, the high intensity was attributed to an enlarged surface area of the roughened Ag electrode, making it possible for more pyridine molecules to attach to the rough Ag surface. Later, Van Duyne et al.[11] and Creighton et al.[12] both reported, after careful characterization of the pyridine molecules and calculations, that the increased surface area was not enough to explain the anomalous increase in the Raman signal. Therefore, they suspected that an additional enhancement mechanism might contribute to the observed enhanced signal. This increase in Raman signal was later recognized as a new phenomenon called surfaced-enhanced Raman scattering (SERS).

There are two generally accepted theories to explain the enormous enhancement, one being the electromagnetic (EM) theory and the other one the chemical (CM) enhancement mechanism. Detailed discussions of each mechanism can be found elsewhere[13], but their main ideas will be presented here.

Classically, an incident oscillating EM field $\overrightarrow{E_0}$ at a frequency ω_L induces a dipole $\overrightarrow{p_0}$ in the molecule that oscillates and radiates at a Raman frequency ω_R. In the linear response approximation, the $\overrightarrow{p_0}$ is linearly linked with $\overrightarrow{E_0}$ and the linear coefficients define the Raman polarizability α_0^R (a tensor due to the vectorial nature of $\overrightarrow{p_0}$ and $\overrightarrow{E_0}$)[14]

$$\overrightarrow{p_0}(\omega_R) = \alpha_0^R(\omega_L, \omega_R)\overrightarrow{E_0}(\omega_L) \tag{1.1}$$

In the case of SERS, several factors are found to contribute to the SERS enhancement by affecting the Raman dipole and its radiation. We can write Equation (1.1) as the following:

$$\vec{p}(\omega_R) = \alpha^R(\omega_L, \omega_R)\overrightarrow{E_{loc}}(\omega_L) \tag{1.2}$$

Where $\vec{p}(\omega_R)$ and $\alpha^R(\omega_L, \omega_R)$ are modified Raman dipole and modified polarizability tensor respectively. $\overrightarrow{E_{loc}}(\omega_L)$ is the local field at the molecular position.

From classical EM theory[14], the radiating power of an surface-enhanced Raman dipole in free space (hence the SERS signal) is proportional to $\left|\vec{p}\right|^2$.

$$I_{SERS} \propto \left|\vec{p}(\omega_R)\right|^2 = \left|\alpha^R(\omega_L, \omega_R)\overrightarrow{E_{loc}}(\omega_L)\right|^2 \tag{1.3}$$

From Equation (1.3), there are two factors that contribute to the SERS intensity: Raman polarizability and local electric field. If either of these two increases, the total intensity of SERS signal will increase accordingly. Therefore, we can identify two types of SERS enhancement: a change in the local electric field $\overrightarrow{E_{loc}}(\omega_L)$, which is referred to as EM enhancement and a change in the Raman polarizability α^R, which is coined as chemical (CM) enhancement.

Strong localized electric field $\overrightarrow{E_{loc}}(\omega_L)$ felt by the molecule can be induced by localized surface plasmon resonance (LSPR). When light is incident on a metal nanoparticle, with a wavelength longer than the nanoparticle's size, the free electrons at the particles' surface will experience a collective oscillation driven by the incident oscillating electric field. When the frequency of the incoming light is close to the intrinsic oscillation frequency of the free electrons, the oscillation will be enhanced and results in LSPR excitation. LSPR leads to large enhancement in the localized EM field in which a molecule can experience, from Equation (1.3), leading to an enhancement of the Raman dipole and hence the Raman signal. Those localized electric fields are

several orders of magnitude more intense than the incident light[14]. This localized region of the intense field around the nanoparticle is called a hot spot. Properties of hot spots will be further elaborated in section 1.3.2 Hot Spots.

While EM enhancement is a general enhancement mechanism, CM enhancement is selective and it is less prominent than EM enhancement. CM enhancement is commonly used to explain the different enhancements among different modes in the same molecule under the same experimental conditions, as well as the perceived difference between experimental enhancements and theoretically calculated results. It arises from the chemical interaction between the molecule and the substrate surface. When a molecule is adsorbed onto the surface, it may form a complex with the metal nanoparticle through a chemical bond. The new bond will result in the change of the molecule's electronic states, leading to a change in the polarizability of the molecule. According to the Equation (1.3), the change of the polarizability will lead to the change of the Raman dipole and the Raman signal. Since the change in polarizability of different modes might not be the same, this results in varying enhancements for different vibrational modes.

It is generally believed that the EM mechanism accounts for the majority of the enhancement while CM mechanism could explain the selected enhanced effect for different vibrational modes. It should be noted that, in a typical SERS environment, it is very difficult to distinguish between CM enhancement and concurrent EM contributions.

Together with the quest to explain the origins of SERS enhancement, researchers find wide applications for SERS. Two limitations need to taken into account. First, only a few metals such as Ag, Au and Cu can yield strong SERS-active substrates[15] due to their dielectric functions having negative real part and small imaginary part in the visible region. Some efforts have been made to study the SERS effect from transition metals[15-16] and from other semi-conductors[15, 17], but the signals are generally much weaker than from coinage metals. Second, the metal surface needs to be rough on the nanoscale after physical or chemical processing, which serves as one of the most important conditions for the substrate to exhibit SERS effect.[16b]

Despite the limitations, the discovery and the development of SERS overcomes the small intrinsic probability for normal Raman scattering process, and it is becoming a very promising tool to probe into the vibrational information of molecular structures. SERS is widely used in fields such as physics[18], chemistry[18a, 19], biology[20], and engineering[21].

1.3 Single-Molecule SERS (SM-SERS)

Since large enhancement (at least~10^8)[22] can be achieved in SERS, the technique is able to detect single molecule. The first observation of single-molecule SERS (SM-SERS) was achieved independently in 1997 by Nie[23] and Kneipp[24]. Both groups claimed to observe the enhancement factor on the order of 10^{14} to 10^{15}. Nie et al. used highly heterogeneous Ag colloidal suspension with rhodamine 6G (R6G) at 2×10^{-10} and 2×10^{-11} M. Comparison between SM-Florescence and SM-SERS was investigated and huge spectral fluctuation in SERS intensities was observed. Kneipp et al. used crystal violet, with a final concentration around 10^{-14} M, absorbed in Ag nanoparticles from a colloidal suspension, excited by near-infrared laser light. They also observed SERS signal fluctuations as well, and by varying the average number of dyes in the scattering volume from 0,1,2 and 3, normalized intensity histograms were constructed. Kneipp et al. claimed SERS intensities histograms obtained for very low concentrations fit a Poisson distribution, which corresponded to the probably to find a small number of dyes in the scattering volume. Kneipp et al. argument was carefully evaluated by Etchegoin et al.[25], who pointed out that the features in the histogram reported by the Kneipp group were simply an artifact due to poor sampling (100~200 measurements taken to construct the histogram). In fact, the features vanish when more measurements (~3000) were performed, the reason being that the enhancement factor inside hot spots is highly varying. Therefore, the idea that the distribution of SERS intensities at SM-conditions follows a Poisson distribution was rejected and since then, there has been considerable research to study SM-SERS statistical behaviors in various contexts[26].

The discovery of SM-SERS allows the study of discrete events from material surfaces with more detailed, vibrational, information. SM-SERS is able to provide a highly resolved vibrational fingerprint of a specific molecule, and compared to SM fluorescence, it is less immune to rapid photo-bleaching. Thus, the SERS field was rejuvenated and literature abounds to study SERS system at SM level.

1.3.1 Enhancement Factor (EF)

In order to compare different SERS substrates (platform that enables SERS), researchers traditionally calculate the enhancement factor (EF). Roughly speaking, the goal is to find substrates with very high EF. The EF is an indication of how much the Raman signal is amplified compared to the normal Raman scattering. First of all, it is very crucial to have a universally accepted definition of EF, so that calculated EF-values can be directly compared. However, many different definitions for EFs are found in the literature, and a more comprehensive study on the EF can be found elsewhere[27]. Two commonly used EF calculations are introduced briefly here:

The first is called single molecule enhancement factor (SMEF) and is defined in Equation (1.4). I_{SERS}^{SM} represents the intensity of SERS signal from a single molecule and $< I_{RS}^{SM} >$ is the average intensity of the normal Raman scattering per molecule. SMEF is used to describe the EF an individual molecule experiences at a particular adsorption site. It is dependent on the orientation of the molecule on the surface and the surface geometry. SMEF is calculated as the ratio between SERS signal and average Raman intensity for the same molecule. It is also approximately proportional to the forth power of the ratio of the local field over the incident field, considering local field enhancement and radiation enhancement[14].

$$SMEF = \frac{I_{SERS}^{SM}}{< I_{RS}^{SM} >} \approx \frac{\left|\vec{E}_{Loc}\right|^4}{\left|\vec{E}_{Inc}\right|^4} \tag{1.4}$$

The second commonly used EF is the average SERS EF (AEF). In a typical experiment, the distribution of SMEF is generally unknown and difficult to calculate. Therefore, it is beneficial to define an EF that represents the average EF of the substrate (taking account the spatial variation) which can be used to compare between substrates. Many studies[28] have focused on this type of determination. The AEF is calculated as:

$$AEF = \frac{I_{SERS} / N_{Surf}}{I_{RS} / N_{vol}} \tag{1.5}$$

Where I_{SERS} is the average SERS intensity, N_{Surf} the number of molecules adsorbed on the surface in the scattering volume, I_{RS} the intensity in a normal Raman situation, and N_{vol} the number of molecules in the probing volume when normal Raman measurements are performed.

Despite the widely adopted EF definitions above, obvious problems arise due to the dependence of the SERS signal in various experimental conditions, including the orientation of the molecule attached to the surface and the different Raman cross section for different molecules. In addition, the calculation of N_{Surf} and N_{vol} in Equation (1.5) has to heavily rely on estimations, which may not be accurate or even comparable in different experimental conditions. Complicating the matter further, even for the same molecule under the same experiment conditions, different bands might have different EFs. This raises the question of which bands are more suitable to be used to calculate EF and to compare among different substrates. Therefore, all these various factors present a significant challenge to define and calculate a meaningful EF value that can be used to compare between substrates.

1.3.2 Hot Spots

As mentioned before, hot spots are the locations considered responsible for the ultrahigh enhancement[29] (factors of 10^8 to 10^9) observed in SERS. They are usually located at the small

junctions between metallic nanoparticles within close proximity or tips or rims of nanoparticles[30], which gives rise to the highly localized EM fields. As Equation (1.3) states, the SERS signal is proportional to the square of the EM field the molecule is experiencing. Therefore, the highly localized EM field means that if the molecule happens to be at the exactly the right place, the signal will be greatly enhanced. In the SM-SERS situation, where there are very few molecules in the scattering volume, and thus, low signal-to-noise ratio, it is generally believed that only the molecules in the hot spot will produce detectable signal, and that the contribution of other molecules is negligible.

The effectiveness of the hot spot for SERS depends on the shape, size and spacing between the metal nanoparticles. Extensive research has been conducted to study the relationship between SERS intensity and different surface morphologies, for instance, nanospheres[19b, 31], nanorods[32] and nanorings[33] etc.

Etchegoin and his group[25a] did a set of studies to understand the characteristics of hot spots. His group concluded that the distribution of EF around a hot spot had a truncated Pareto distribution and, at full coverage, 98% of the total SERS signals would arise from only 2% of the molecules on the surface of a single dimer.

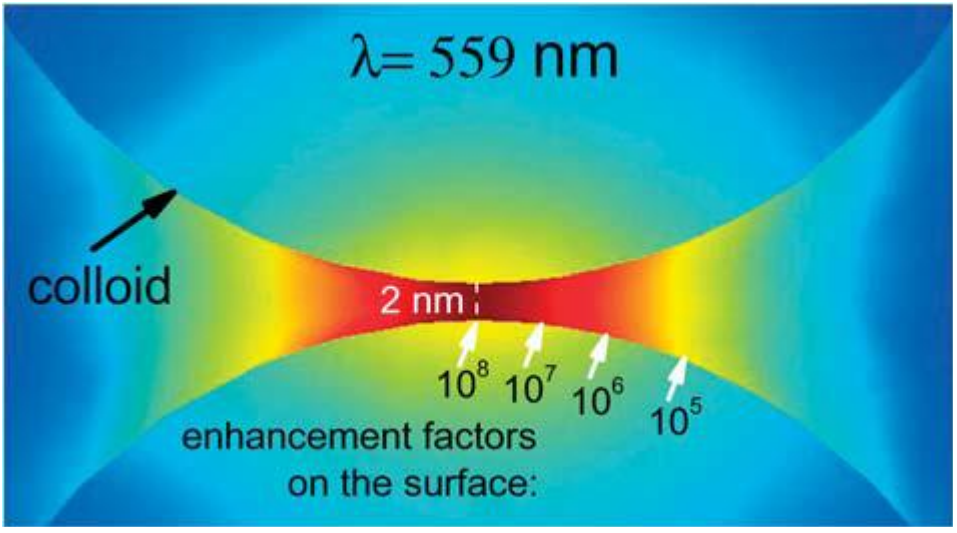

Figure 1.1 Calculated EF distribution in a typical hot spot between two Au colloids
(Reproduced from Ref. 34 with permission from the PCCP Owner Societies)

Furthermore, the maximum EF is located at the center of a hot spot and the EF decays exponentially from the center. Figure 1.1 shows the EF distribution[34] in a typical hot spot excited by 559 nm laser calculated using electrostatic approximation with finite-element modeling. The hot spot is formed by two Au colloids with 30 nm diameter and 2 nm apart from each other. Figure 1.1 shows that in the center of the gap, EF can reach as high as 10^8 but when moving farther away from the center, EF drops exponentially to 10^5, where it is only several nanometers away from the maximum EFs. In a typical SM-SERS experiment, the contribution from EF smaller than 10^5 can be ignored therefore[25a], only a very small region around the center of the hot spot gives rise to the majority of the Raman signal. This corroborates the idea that the majority of the SERS signal arises from only a very small fraction of the molecules and that molecules outside the hot spot contribute very little. Therefore, there is a good reason to just consider molecules in the hot spot region, since they dominate the overall signal.

Another consideration is that EFs for different hot spots within a laser illuminated area are not the same. In fact, they may differ by several orders of magnitude, due to different resonances (excitation wavelength), differences in gap distance between metallic nanoparticles, and differences in sizes or shapes of the nanoparticles[25a]. Therefore, when we model the signal under the illuminated area to be the sum of the enhancement effects of all the hot spots, special treatment, such as weighted factors, needs to be taken into account, because hot spots themselves are not homogeneously enhancing the signal.

1.3.3 Bi-analyte technique

Even though SM-SERS has received much attention, since the first claim in 1997[23], researchers have debated whether the observed effect was really from single molecules or rather than other effects or artifacts. In 2002, Doering and Nie[26b] pointed out that surface diffusion (molecules coming in and out of the regions where electric fields are highly localized, i.e. hot spots, getting adsorbed or desorbed rapidly) is responsible for the temporal fluctuations of SM-

SERS signals (i.e. blinking behavior). However, the idea was challenged by Anderson et al.[35], and they argued that blinking associated with the nanostructure is more likely than with the adsorbate because they observed blinking behaviors independent of the presence of adsorbates.

In 2005, Le Ru[36] et al. proposed to use a new technique - bi-analyte technique - to solve the long-standing debate about the reality of SM-SERS. Instead of using one kind of molecule with ultralow concentration, and relying on the very few events with low signal/noise ratios, a mixture of two kinds of molecules were used at the same time with relatively high concentration. When the two compounds have comparable Raman cross section, comparable adsorbing/desorbing rate, and spectrally resolved distinct peaks, then spectral fluctuations could be attributed to either or both molecules. This eliminates the alternative explanation for the SERS blinking, such as photo-oxidation and modification of the nanostructures on the surface. This technique is generally accepted as the definite proof of SM-SERS and enhances the understanding of this phenomenon a great deal.

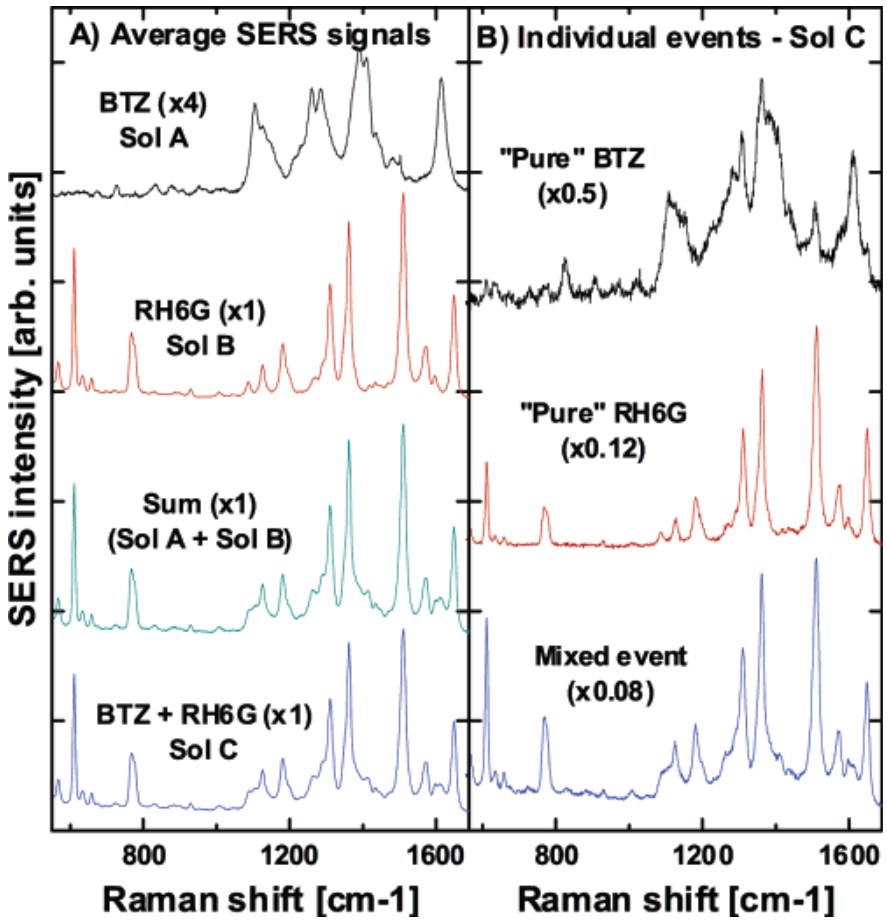

Figure 1.2 Bi-analyte technique to prove SM-SERS

(Reprinted with permission from Ref 36. Copyright 2006 American Chemical Society)

There are two experiment approaches to obtain SERS signals. One of them uses a colloidal suspension with a small scattering volume. Fluctuations in the SERS intensities are observed against time from the constant diffusion of colloids in and out of the volume being probed by the laser. The other approach uses dry substrates. In this case, SERS mapping is performed across a pre-determined area on the substrate and spatial variations in SERS intensities are obtained.

In their original work, Le Ru[36] et al. used Ag colloidal suspension and benzotriazole dye (BTZ) and R6G as the probe molecules. Solution A was 100 nM BTZ, solution B was 100 nM R6G and solution C was the 100 nM mixture of both dyes. Figure 1.2 shows that when the spectra from solutions A and B were added, an identical spectrum of solution C, within

experimental error, was obtained. The temporal evolution of the spectra of the mixture, presented in Figure 1.2B, shows pure BTZ and pure R6G events as well as mixed events. This clearly shows that the SERS signal originated from the dyes going in and out of the hot spots. In some events, only BTZ molecules gets adsorbed into the hot spot region, yielding pure BTZ events (spectra with only BTZ signals). On the other hand, in some events, only R6G molecules gets adsorbed onto the hot spot region yielding pure R6G events (spectra with peaks specific to R6G). In rare occasions, both dyes visit hot spots simultaneously leading to mixed events. This technique employs higher concentration (100 nM) than previous studies (less than 1 nM), and therefore, it does not heavily rely on the estimation of the molecule/colloid ratio, which is problematic in the previous analysis of SM-SERS experiments.

The bi-analyte technique has received much attention and it has been regarded as the first technique to provide direct evidence of SM-SERS. However, the application of the technique is complicated if two dyes with different chemical structures are used. Dyes with different chemical characteristics have different Raman cross sections, absorption spectra and abilities to bind on the surface. These differences would induce a layer of bias (in favor of the dye that adheres better on the surface, for instance) in the recorded data, affecting the assumption that dyes with the same concentration are equally competitive in terms of locating the hot spots. Pettinger et al.[37] also points out that the different Raman cross sections and other chemical properties need to be considered and compared in order to understand the SM-behavior further.

The ideal situation in the SM-SERS bi-analyte technique is that the two types of dyes can be spectrally well resolved (i.e. have distinguishable Raman features), but present the same chemical properties (binding abilities to the surface, Raman cross section etc). Etchegoin et al.[38] achieved this ideal situation by isotopic editing. They synthesized d4-R6G by substituting four hydrogen atoms of the phenyl moiety in the R6G molecule with deuterium atoms. After a full characterization, the isotopically edited d4-R6G and un-edited R6G pair served as an ideal SERS probe partners for bi-analyte SERS. R6G and d4-R6G have i) comparable Raman section for

most modes; ii) very similar chemical properties in terms of surface affinity; iii) chemical enhancement on the same order of magnitude; iv) distinguishable Raman spectra. d4-R6G has distinct peaks in the 600 cm^{-1} to 640 cm^{-1} region and 1300 cm^{-1} to 1390 cm^{-1} region, arising from C-D stretching[26a]. The isotopic editing pushed the bi-analyte technique to another level with the ideal probes to provide abundant information in the SM-SERS statistics.

1.3.4 Statistics of signals

Due to the long-tail (truncated Pareto) EF distribution around a hot spot and large variations across different hot spots under laser illumiation, different statistical behaviors (shapes of histograms) of the SERS signal fluctuations can be seen depending on the surface coverage.

Ethegoin et al.[25a] performed Monte Carlo simulations to demonstrate the changes in statistical behaviors of the intensity histogram with the surface coverage for a single dimer. In the simulation, the number of molecules (N_{mol}) randomly positioned on the surface of a dimer was varied. The EF distribution around the hot spot was previously obtained (truncated Pareto distribution), and 10,000 configurations/events were considered during the simulation.

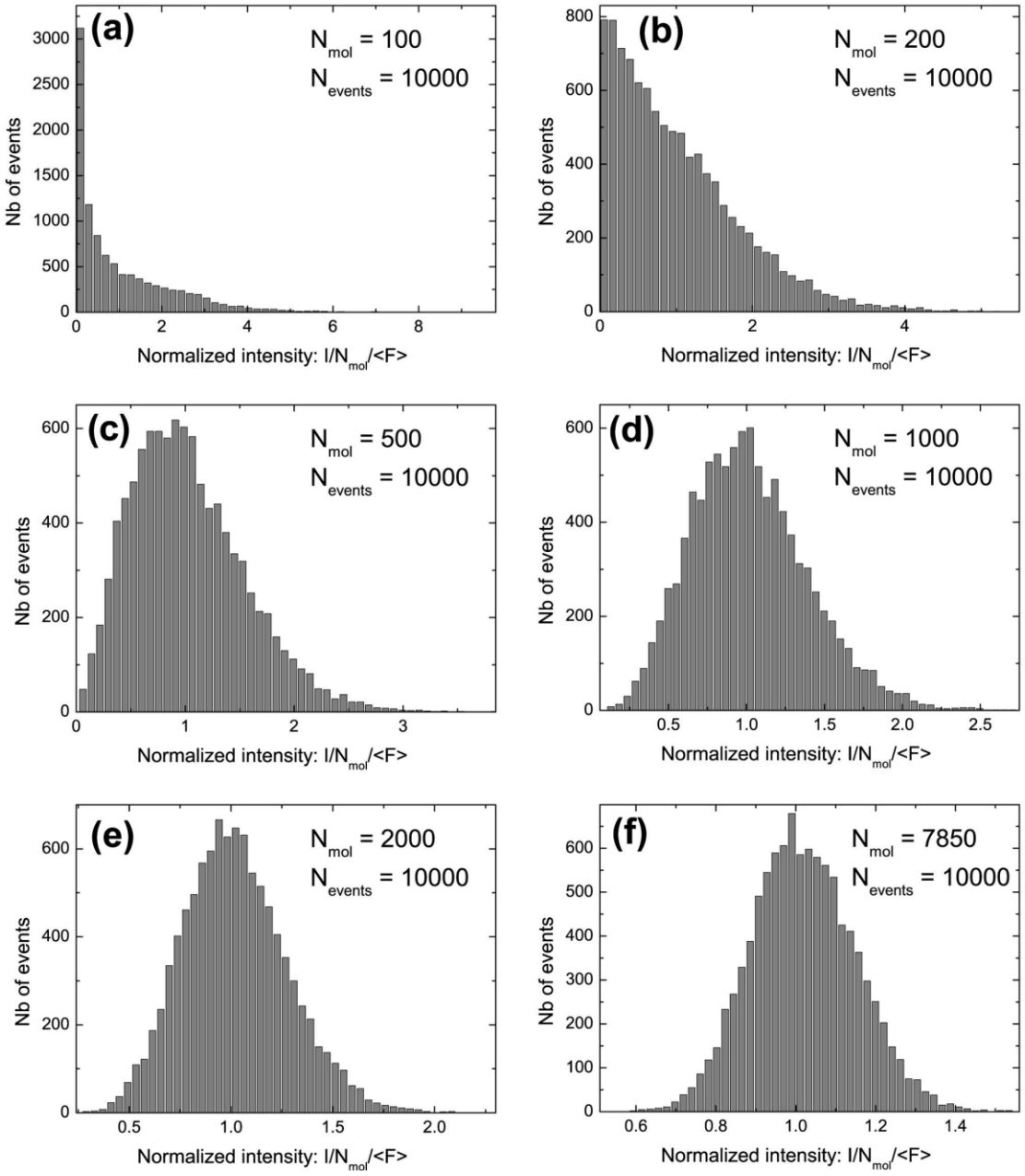

Figure 1.3 Intensity histograms of Monte Carlo simulation of normalized SERS signal from different number of molecules (Nmol) on the metal surface.

(Reproduced from Ref 25a, with the permission of AIP Publishing)

The trends observed by Etchegoin et al. are shown in Figure 1.3. In the low surface coverage (hence low concentration of the molecules) situation (Figure 1.3 (a) and Figure 1.3 (b)), a large number of null events are expected. At low surface concentrations, the probability of a molecule

to adsorb in the (small) hot spot region is low. In very rare cases, the location of the adsorbed species happens to be in a hot spot with a large EF, leading intensities much larger than the average. This corresponds to the large fluctuations (temporal or spatial) observed in real SERS experiments at low solution concentrations. The shape of the histogram is then a long-tail distribution due to the highly localized hot spots. The situation shown in Figure 1.3 (a) and Figure 1.3 (b) is then coined "low concentration regime" or "SM regime"[25a].

When the surface coverage increases (so does the concentration of dyes in solution), a gradual change is observed in the shape of the intensity histograms; from a long-tail distribution to a non-symmetric Gaussian-like distribution. The probability of observing large intensity (relative to the average) events is now small in Figure 1.3 (c),(d) and (e). The truncated Pareto distribution of enhancements accounts for the high intensity tail that always exists even in relatively large surface coverage. Only when the number of molecules on the surface is extremely large (closer to a monolayer), that the long tail vanishes and a Gaussian distribution (Figure 1.3 (f)) is revealed. Also note that the higher the surface coverage, the narrower the Gaussian curve, because less fluctuation is expected and the exchange of molecules between the solution and the surface has a less impact on the overall SERS signal. This situation is coined "high concentration regime" or "average-SERS regime".

1.4 Research Objective

As described in 1.3.1 Enhancement Factor (EF), the use of EFs to compare different SERS substrates has some limitations, since they are highly dependent on many factors, such as experimental conditions, orientation of the molecule attached to the surface, Raman cross sections, estimations of the number of molecules on the surface, and different EF for different Raman bands. There needs to be more universal and comprehensive approaches to compare the efficiency of SERS substrates.

Several criteria can be adopted to evaluate a SERS substrate more comprehensively rather than a simple EF value estimation. In principle, a good SERS substrate should contain hot spots 1) of high density, 2) of high enhancement with 3) a low variation in their enhancement abilities and it should have 4) a high repeatability and 5) exhibit Gaussian distribution in their intensity histogram at a lower concentration. The first four criteria are easy to understand and the last one needs a bit more explanation.

Considering an ideal SERS substrate (this is not a real case, just a thought exercise) which have equally good hot spots with high enhancement everywhere on the surface. If a SERS measurements is taken, a detectable signal will be obtained even if there is only one molecule absorbed on the surface. Furthermore, no matter where the molecule is absorbed, the same signal intensity is obtained due to the homogeneity of hot spots. One molecule is the lowest surface concentration achievable in an experiment. Now, in a real case, the best substrate should still exhibit "average-SERS behavior" (Gaussian distribution of intensities) even at low concentrations. This serves as one of the two guidelines to be further discussed in Chapter 3 Analysis and Discussion.

The advantages of using these criteria are: i) it serves a more legitimate way to compare different substrates than simply comparing estimated EFs; ii) surface coverage is not needed, and only the solution concentration serves as the experimental parameter; iii) allows for comparison between different kinds of substrates, such as colloidal suspension and supported nanostructures; iv) difference in the signal due to molecular orientation is eliminated in the statistical treatment. v) These criteria evaluate different aspects and they are able to provide more comprehensive information about a certain substrate.

This research project focuses on using those five criteria above to evaluate different SERS substrates. Instead of comparing EFs, SM-SERS and average-SERS behaviors are investigated for each substrate by changing the solution concentrations of the dye. In that case, substrates are

compared by way of analyzing the changes in the intensity histograms for different solution concentrations of the dye probe, ranging from SM regime to average-SERS regime.

The five criteria chosen, the specific metrics to quantify those criteria, and a more detailed discussion on the substrate comparison will be found in Chapter 3 Analysis and Discussion .

1.5 Organization of the thesis

This thesis is organized into four chapters. Chapter 1 provides general background about the field of SERS and sets the current work in context. Chapter 2 focuses on the experimental details of the thesis, including the principles and procedures to perform nanosphere lithography and corresponding scanning electron microscopy (SEM) images, UV-vis extinction spectroscopy and SERS experiments. It also provides details on how the raw Raman data were processed through background removal and principal component analysis (PCA). PCA results are also provided. Chapter 3 furthers the discussion on what makes a good substrate by proposing five criteria and six quantification methods. A detailed analysis and comparison between substrates are provided. Chapter 4 will follow with final remarks and conclusion.

Chapter 2 Experiment details and results

This chapter provides a detailed account of the fabrication of SERS substrates, SERS experiments, data analysis technique and results.

.

2.1 Nanosphere Lithography (NSL)

2.1.1 NSL procedures

There has been great effort to fabricate nanostructures described in the literature. Metallic nanostructures serve as SERS substrates used in many different areas of study, including optics[39], surface chemistry[40], and thermodynamics[41]. Despite the large number of fabrication methods available, researchers are still trying to optimize the methods in order to achieve highly reproducible and cheap to fabricate nanostructures, while maintaining control over the nanostructures shape, size and interspacing on a large scale. Among all the methods, nanosphere lithography (NSL), introduced to the field of plasmonics and SERS by Van Duyne et al.[42], has received considerable attention. It is a simple, fast and cheap way to fabricate nanoparticles with tunable sizes, shapes and interspacing parameters. A large number of structures have been fabricated by NSL and their properties[43], such as their localized surface plasmon resonance (LSPR) response and its sensitivity to the external nano-environment[44], have been studied.

The experimental procedure for NSL is detailed in Figure 2.1.

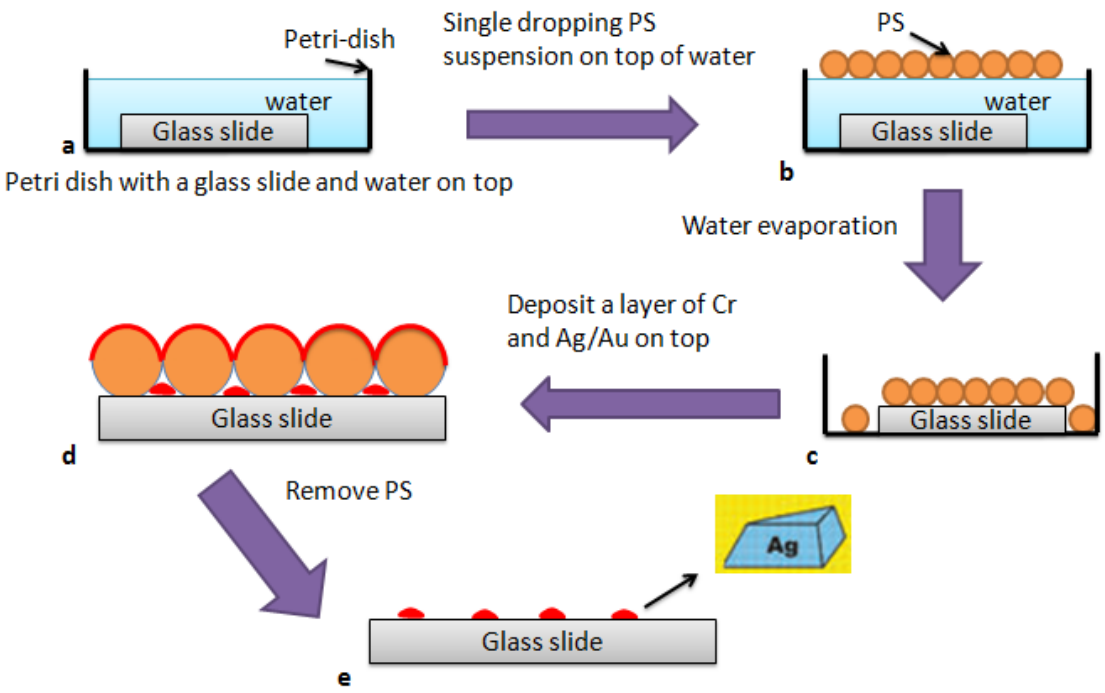

Figure 2.1 Schematic procedure for performing NSL

The NSL procedure has several steps as indicated below:

Step (a): Glass slides are rinsed and cleaned in piranha solution (3:1 concentrated H_2SO_4 : 30% H_2O_2) for half an hour and washed with ultrapure water (USF Elga, Maxima, model Scientific MK3, ρ_{water} =18.2 MΩ cm). They are then sonicated 3 times for 10 minutes. After cleaning, they are either immediately used or stored in ultrapure water.

Step (b): Three different diameters (372 ± 10 nm, 505 ± 8 nm, 746 ± 2 nm) of monodisperse suspensions of polystyrene (PS) nanospheres (from Polysciences, Inc.) are diluted with ethanol (1:1 v/v). Single drops of the resultant mixture are cast slowly and carefully on top of water in a petri-dish; glass slides are submerged under the water. The PS nanospheres self-arrange to find the most favorable configuration with the lowest energy, thus forming a hexagonally patterned, densely packed single layer on top of the water.

Step (c): The water is allowed to evaporate (it might take 36 hours) and the nanospheres are drawn closer together due to capillary forces, crystallizing on the glass slides in a nicely arranged pattern. The pattern serves as the mask for subsequent metal deposition.

Step (d): 5 nm thick Cr adhesion layer followed by a layer of 40 nm thick Ag or Au is deposited thermally over the mask. The metals cover the top of the PS nanospheres and also fill the gaps between them, leading to triangle-like nanoparticles. The depositions were done using a Kurt J. Lesker PVD 75 thermal and electron beam evaporator available at the 4D lab at Simon Fraser University.

Step (e): The substrate is immersed into toluene and sonicated for 30 s to remove the nanospheres from the surface. The metallic layer on top of the nanospheres is washed away due to the removal of nanospheres, but those metal nanoparticles in the gaps between nanospheres remain as well-arranged pattern.

Nanospheres with different sizes were used and that dictates the ultimate size and spacing of the triangle-like nanoparticles.

The Van Duyne group has made considerable efforts to systematically characterize the SERS properties of Ag substrates developed by NSL[45]. This includes correlating the EF factors with LSPR extinction wavelength. The maximum EF was estimated to be $> 1\times10^{8}$. Numerical simulations[46] have also been performed to yield the distribution of electric field squared, averaged between 0 and 2 nm from the nanostructure , as shown in Figure 2.2. The color bar is the logarithm of the induced electric field compared to the incident field. Figure 2.2 indicates that the induced field is very small in most of the surface, but the induced field becomes larger when moving towards the edges at the bottom of the nanostructure. The field increases exponentially until it reaches the tip of the edge, reaching 12,000 times enhancement relative to the incident field. Equation (1.4) states that the SMEF is proportional to the forth power of the ratio of the localized field to the incident field; therefore it is expected that molecules adsorbed onto the tip of edges make the most substantial contributions to the overall SERS signal. A more comprehensive

study of electric field distribution around Ag triangular nanoparticles can be found elsewhere[47], where the optimal EF is estimated to be 10^{10}. The surface roughness of each individual nanoparticles is also likely to contribute to the overall enhancement. In addition to theoretical study, experimental evidence[48] has also been provided to confirm that the large enhancement actually comes from the sharp tips of triangular nanoparticles. All of the literature above shows that SERS substrates fabricated using NSL methods are capable of being used to investigate the SM-SERS phenomenon, because the EF factors are sufficient enough to probe SMs [49].

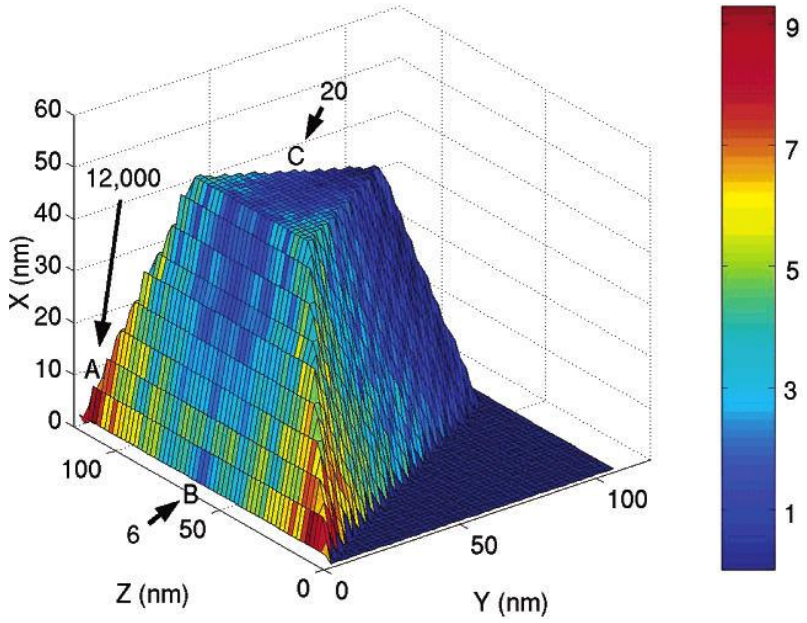

Figure 2.2 Distribution of electric field squared, averaged between 0 and 2 nm from the nanostructure. The color bar on the right is the logarithm of the ratio of the induced electric field over the incident field

2.1.2 Substrates Used In This Thesis

As seen in Figure 2.1, the triangular-shaped nanoparticles have different sizes and spacings, controlled by the diameter of the PS nanospheres. In this thesis, three different sizes (diameters) of PS nanospheres were used: (372 $\pm$10) nm, (505 $\pm$8) nm, (746 $\pm$2) nm, followed by Ag or Au deposition. Therefore, there are six different substrates in the experimental data set, and their labels, summarized in Table 2.1, will be used throughout the thesis.

Table 2.1 Labels for the different substrates

PS nanosphere diameter /nm	Au deposition	Ag deposition
372 ±10	Au3	Ag3
505 ±8	Au5	Ag5
746 ±2	Au7	Ag7

2.1.3 SEM Characterization

All the substrates were mounted on a clamp stub (from Ted Pella) and imaged with a Hitachi field emission S-4800 scanning electron microscope (SEM) with an accelerating voltage of 1kV , emission current 10 μA, working distance 8 mm and the mix (secondary and backscatter electrons) detector.

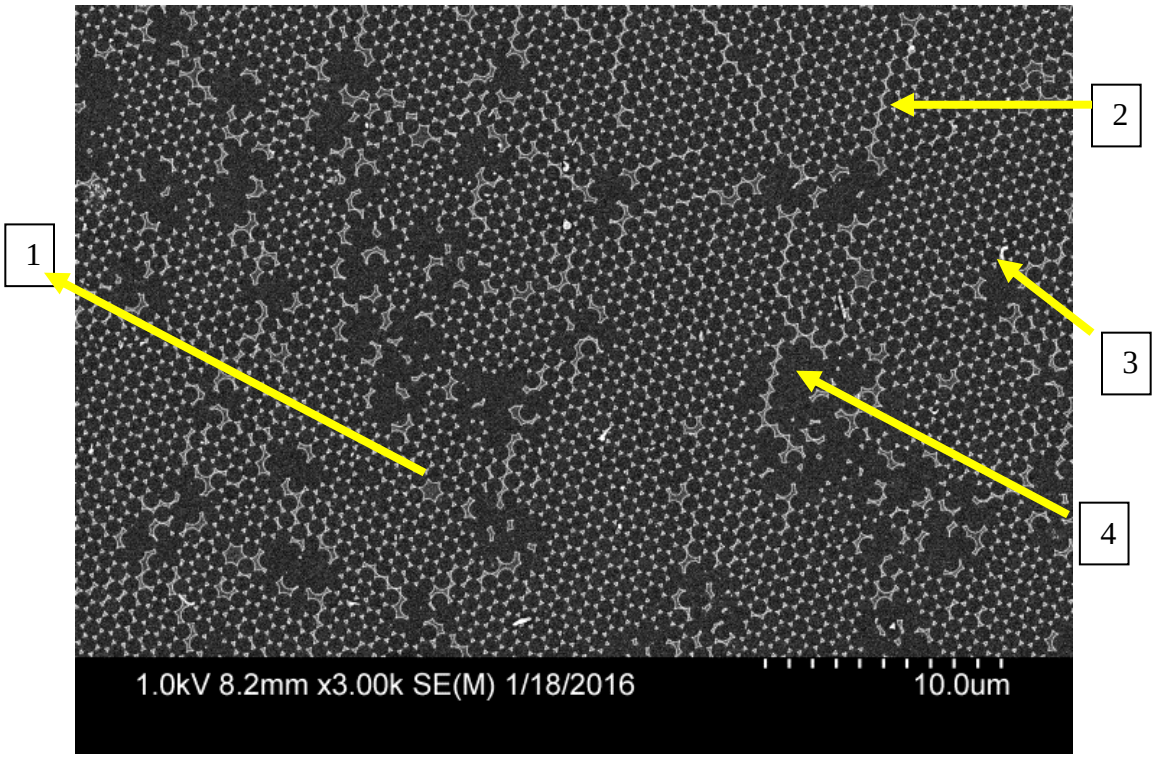

Figure 2.3 Typical SEM image of Au7 on a large scale. The fabrication defects are indicated by the arrows

Figure 2.3 shows a top view of substrate Au7. For the large part, the triangular nanoparticles were well arranged, leading to organized structures, except for a few defects. Site 1 (labeled in Figure 2.3) represents the absence of one PS nanosphere in the masked region. Site 2 results from the dislocation of PS nanospheres in the packing, with the continuous long Au peninsular shape of structure marking the boundaries of different domains of arrangement. Site 3 results from contamination of the substrate. There also exists black areas, as indicated by site 4, where the nanoparticles have been washed away by sonication. All the other substrates with masks of 746nm or 505nm-diameter PS nanospheres reveal similar periodic structure of the nanoparticles and defects in their arrangement. The results from Figure 2.3 agree with similar work in the literature[48, 50].

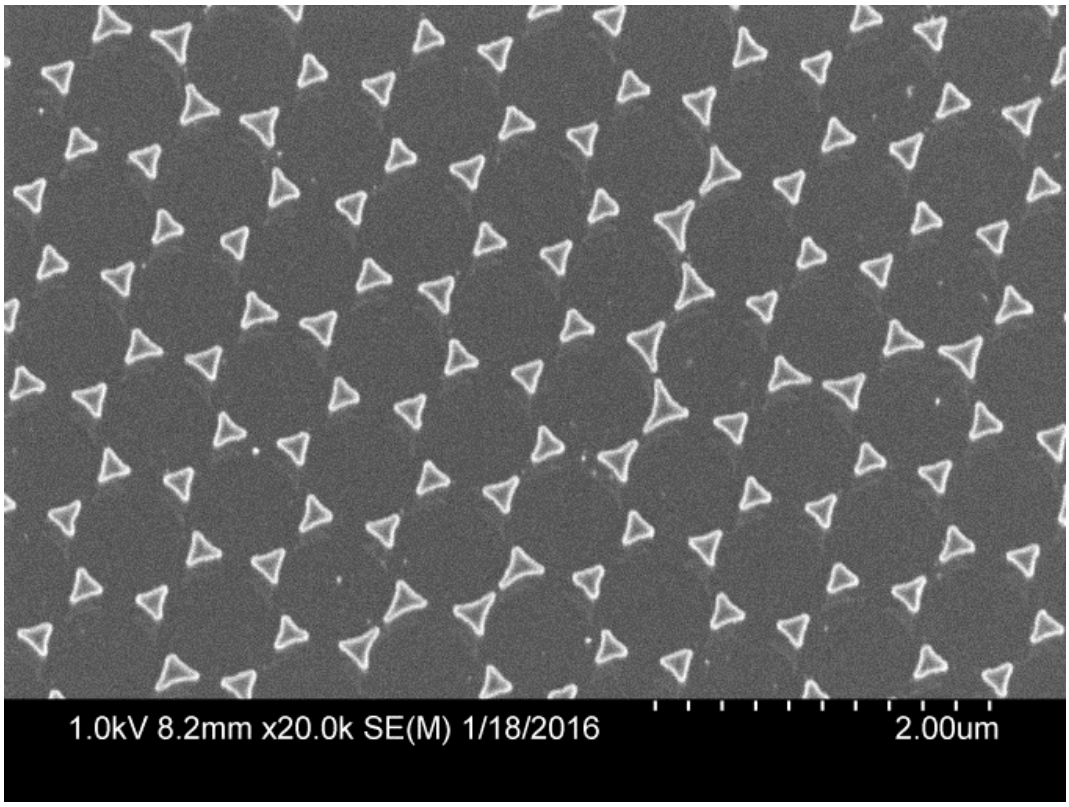

Figure 2.4 Typical SEM image of Au7 on a smaller scale, emphasizing the well-arranged triangular nanostructures

Figure 2.4 is a zoom-in image of part of Figure 2.3. Clearly, the triangular nanoparticles are well arranged and of approximately equal size and shape in this region. Slight variations in nanoparticle geometry are likely due to the slight shift in the arrangement and the small size distribution of PS nanospheres.

Figure 2.5 shows a top view of Au3 substrate. Many defects are present causing a low level of periodicity in nanoparticle arrangement. The same was observed to Ag3 substrate as well, which is likely due to the increasing difficulty to form a well-arranged PS pattern for nanospheres of small diameter .

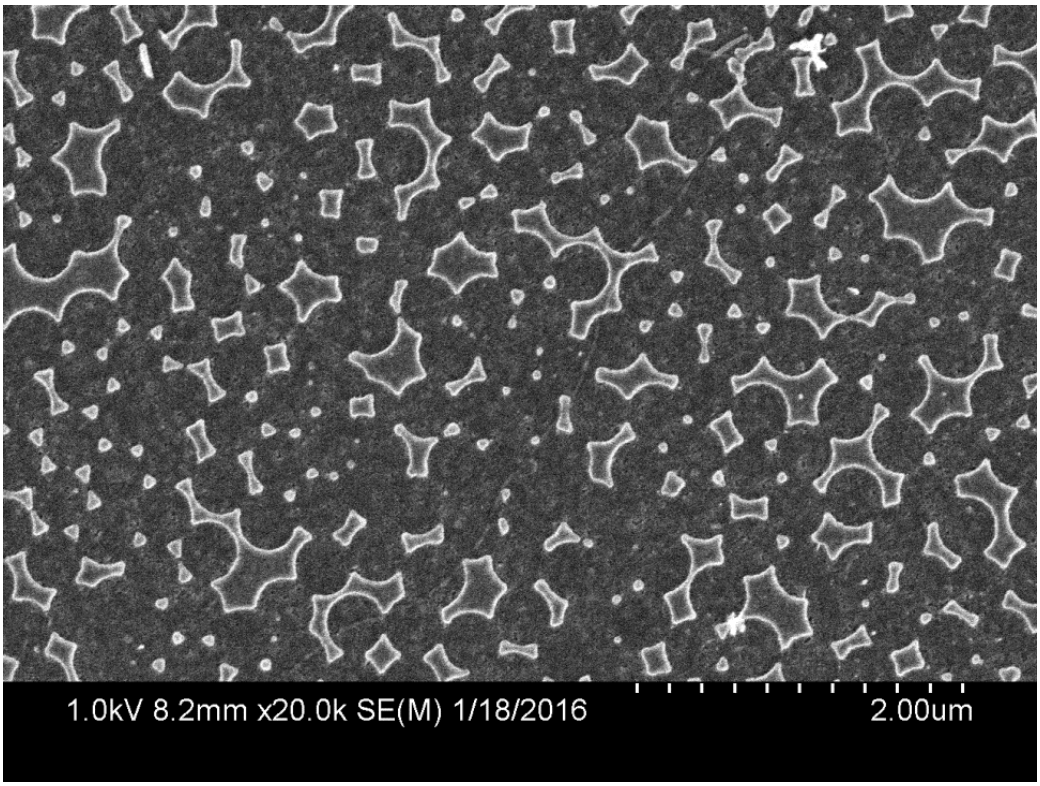

Figure 2.5 Typical SEM image of Au3 with few periodic triangular remains

Table 2.2 summarizes the size of the nanoparticles and inter-particle spacing for different substrates as estimated from the SEM images. The nanoparticle dimensions for the 505 nm diameter mask were approximately 100 nm with 150-200 nm distance from their nearest neighbors. Larger particles (approximately 200nm) with the distance of 100-200 nm between

them, result from the 746 nm-diameter mask. Similar estimations were not done for Au3 and Ag3 substrates (372 nm diameter mask), since the substrates contained few noticeable patterns and large defects were present across the whole substrate (Figure 2.5). SEM images show no noticeable size differences between Ag and Au nanoparticles. In other words, the size and shape of the nanoparticles depended on the mask diameter, regardless of which metals were deposited.

Table 2.2 Summary of size and inter-particle spacing between triangular nanoparticles obtained from masks with PS spheres of different diameters

Diameter of PS spheres /nm	Size of Triangular Nanoparticles /nm	Inter-particle spacing (tip-tip) /nm
505 ±8	~100	150-200
746 ±2	~200	100-200

From theoretical calculation, electromagnetic coupling is substantial if the two nanoparticles are within the distance of 50 nm[50]. However, the spacing between nanoparticles in all of the substrates are much larger than 50nm, resulting in negligible electromagnetic coupling between particles. Therefore, the EM enhancement stems largely from each individual un-coupled particle[44].

2.2 UV-vis extinction spectroscopy characterization

Characterization of substrates is particularly important to understand their SERS performances. One of the most often adopted approaches is UV-vis extinction spectroscopy, which is widely used in the literature to characterize the optical properties of a substrate[51]. When light is incident on the surface, two processes, i.e. scattering and absorption will take place that lead to the reduced amount of intensity of the transmitted power. UV-vis extinction spectroscopy,

therefore, measures the wavelength dependence ability of a particular substrate to “extinct” the transmitted light power [14].

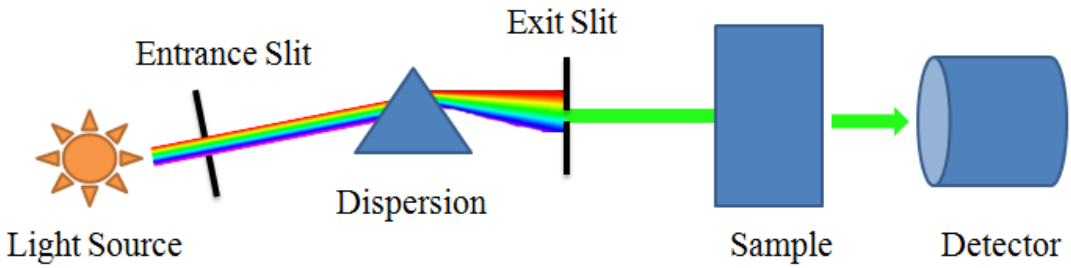

Figure 2.6 Schematic overview of UV-vis spectrometer

Extinction spectra were recorded by a USB4000 UV−vis spectrometer (Ocean Optics, Beckman Du 7500) with the spectral range from 350 nm to 1000 nm at room temperature in air. The background was set using the spectrum of a clean glass slide. Figure 2.6 the schematic overview of UV-vis spectrometer. Light of different wavelength comes out from the source and goes through the entrance slit, gets dispersed by prisms or other dispersion devices. Exit slit is orientated to only allow light with a specific wavelength to pass. When the light passes through the sample, the sample absorbs and scatters the light, resulting in light transmitted with less intensity. The light intensity is detected by the detecting devices, which are connected to the computer that compares the intensity with the previously set background spectrum and displays the results on the screen.

The peak of UV-vis extinction spectroscopy indicates the resonance at a particular wavelength in terms of LSPR, which serves as the basic EM principles of the SERS enhancement (see 1.2 Surface-Enhanced Raman Scattering (SERS) for more details) . Therefore, the resonance peak of UV-vis extinction spectroscopy generally correlates with the maximum SERS enhancement on the surface with respect to laser excitation wavelength[52], although the correlation is not precise in some cases[53].

Figure 2.77 shows the UV-vis extinction spectra of all the substrates. It can be clearly seen that every substrate exhibits a peak in its extinction spectrum in the visible region, which is one of the characteristic of LSPR effects of noble metal nanoparticles[54]. The HeNe laser excitation wavelength, 633 nm, is also indicated in Figure 2.77.

Au3 (color pink) has a small peak at 618 nm with a FWHM 101 nm; Au5 (color green) has a broader and larger peak at 677 nm with a FWHM 118 nm; and Au7 (color dark blue) has a peak at 688 with a FWHM 197 nm. The peaks are red shifted as the size of nanoparticles increases and this is in good agreement with literature[42]. The excitation wavelength (633 nm) falls somewhere in the shoulders of the extinction profile for all of the Au substrates and it is hard to judge which one will have the highest SERS enhancement since the extinction profile only provides qualitative information[53].

Ag3 (color black) has a peak at 470 nm with a FWHM 135nm, Ag5 (color red) has a peak at 485 nm with a FWHM 140nm and Ag7 (color light blue) has a peak at 888 nm with a FWHM 200 nm. Similar to Au substrates, as the size of nanoparticles increases, the peaks are shifted to the right and the shifts are in good agreements with literature[44]. However, again, none of those peaks are near 633 nm excitation wavelength and no qualitative explanation can be drawn from UV-vis extinction spectra.

More thorough understanding of each of the substrates' behaviors can be gained through the performance of computational simulations, such as coupled dipole approximation (CDA)[55], but these simulations were not performed in this thesis.

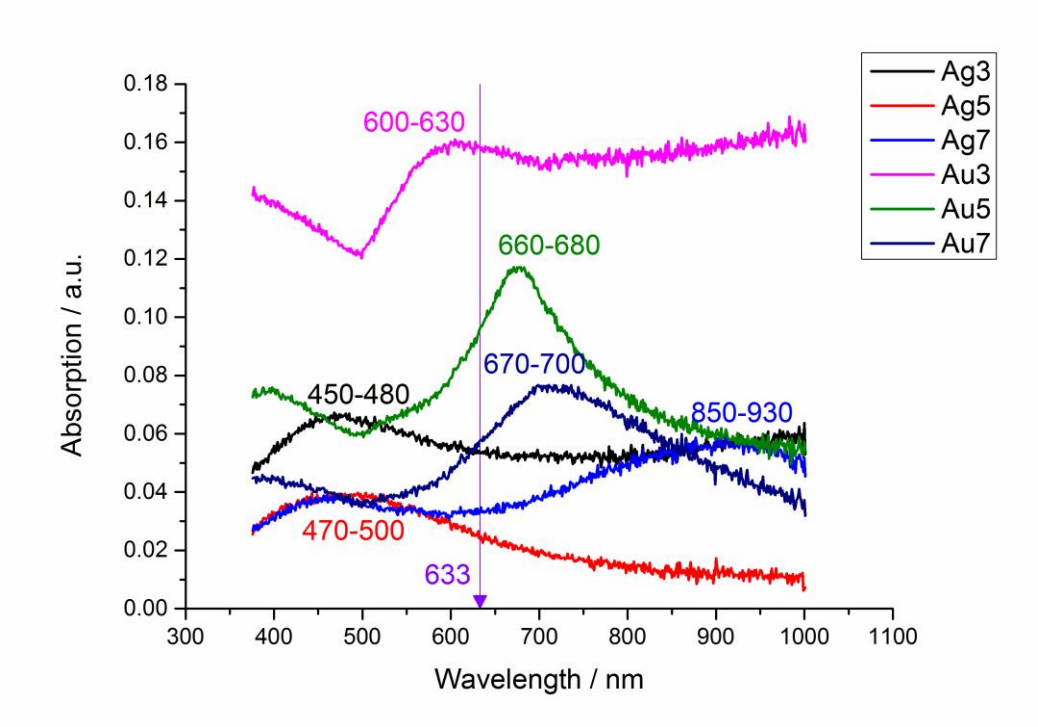

Figure 2.7 UV-vis extinction spectra of all the substrates with violet arrow indicating the position of 633nm HeNe laser excitation

2.3 Rhodamine 6G (R6G)

Rhodamine 6G (R6G) is a dye widely used as a SERS probe due to its large Raman cross section[27]. It is a cationic dye that could adsorb easily onto the negatively-charged surface of metallic nanoparticles due to electrostatic attraction[56]. Its molecular structure is shown in Figure 2.88. Other ways of bonding to the metal surface (e.g. through N-Ag bond formation[57]) are also proposed.

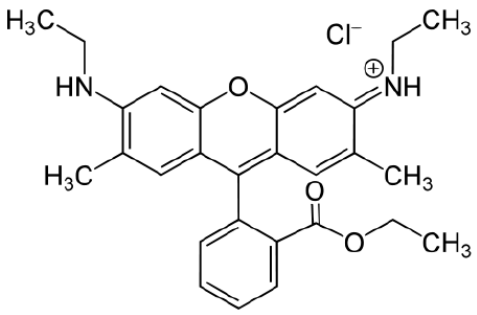

Figure 2.8 Chemical structure of R6G

The thesis focuses on the Raman shift of R6G in the range of 1200 cm^{-1} to 1800 cm^{-1}. Table 2.3 shows the typical bands and their assignments.

Table 2.3 Selected vibrational bands and their assignments[57-58] for R6G in the Raman Shift range between 1200 cm^{-1} and 1800 cm^{-1}.

SERS bands /cm^{-1}	Assignment
1271	C-O-C stretch
1312	In plane xanthene ring breath, N-H bend
1365	Xanthene ring stretch, in plane C-H bend
1509	Xanthene ring stretch, C-N stretch, C-H bend, N-H bend
1572	Xanthene ring stretch, in plane N-H bend
1650	Aroma C-C stretch, in plane C-H bend, xanthene ring stretch

All the SERS experiments were conducted using R6G (CAS 989-38-8, Sigma-Aldrich) dissolved into ultrapure water. Sequential dilution was performed for all R6G aqueous solutions with various concentrations. Detailed description of R6G solution preparation can be found in 2.4.3 SERS experiments

2.4 Raman Instrumentation

2.4.1 SERS cell design

A SERS cell made of Teflon was fabricated to act as a platform for all the SERS measurements. The side view of the SERS cell used in the experiments is shown in Figure 2.99. Two Teflon pieces, secured together by a screw set on each side, make up the main body of the cell. The bottom piece has a 1 inch by 1 inch hole in the centre, allowing enough room to place the SERS substrates (nanoparticles fabricated as indicated in 2.1 Nanosphere Lithography (NSL), on top of a 1 inch by 1 inch glass slide). The top piece has a round hole through the centre with a larger concentric circular hole at the bottom designed to fit in a rubber O-ring. When the screws bring the two Teflon pieces together, the top piece presses the rubber O-ring against the bottom one to prevent leaks. Solution of R6G (total volume between 1 to 2 mL) was dropped using a pipette into the hole of the top substrate for SERS experiments.

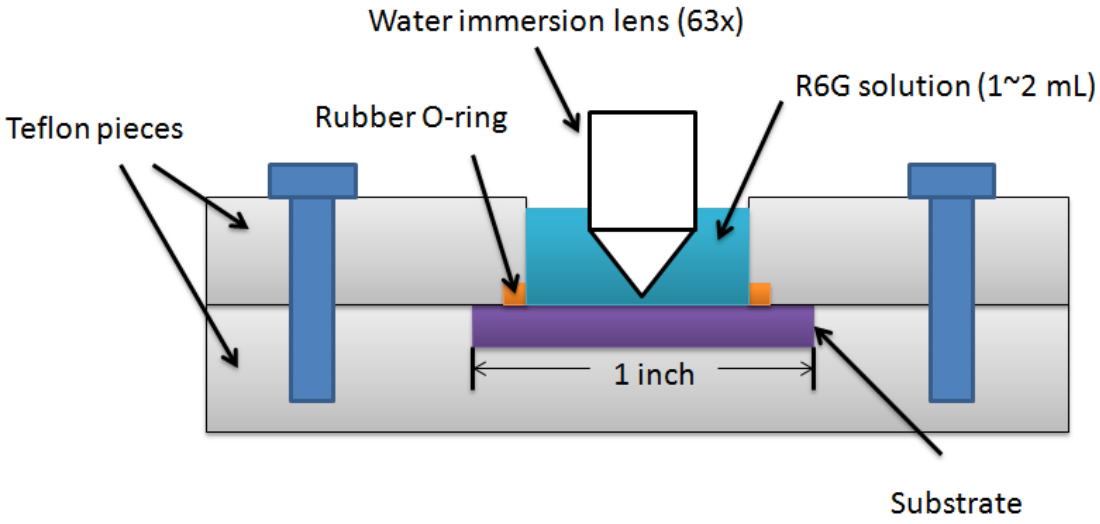

Figure 2.9 Side view of the cell used in SERS experiments

The mounted cell was placed on the translational stage of the Renishaw Raman system for SERS measurements. After the experiments, the Teflon pieces of the cell were immersed in Piranha solution (H_2SO_4 : H_2O_2 = 3:1) for 24 hours for cleaning. This procedures eliminates any possible organic contamination.

2.4.2 Renishaw Raman system

SERS measurements (in the range of 1200 cm^{-1} to 1800 cm^{-1}) were performed using a Renishaw in Via Raman system (Renishaw Inc., Hoffman Estates, IL). Figure 2.1010 shows the schematic set up for the system. A He-Ne laser at 632.8 nm wavelength was used as excitation source. The beam was directed to this system by several optical mirrors and finally focused on the surface of the substrate with 63x water immersion lens (N.A.=0.9). Then the same objective lens collects the back-scattered light and directs it to the Notch filter where elastic Rayleigh scattering light is removed and only inelastic Raman scattering light is left and directed to the focusing optics and grating. The Raman spectra are recorded by the CCD camera. In this thesis, only the Stokes shift was measured.

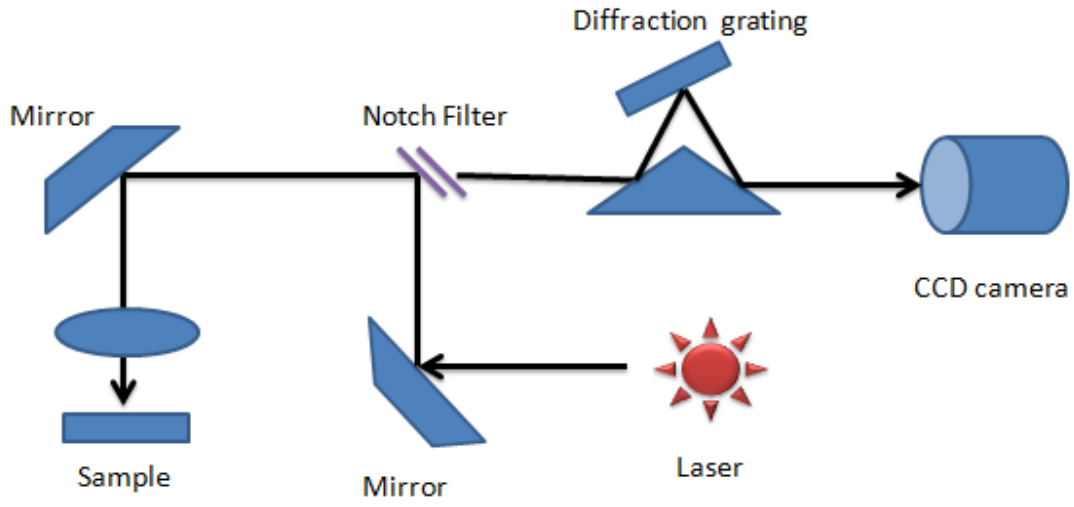

Figure 2.10 Schematic overview of the Raman system

2.4.3 SERS experiments

All the SERS experiments were performed under the same experimental conditions: 632.8 nm laser beam as the excitation source (warmed up for more than 1h before each experiment); a 63x water immersion lens (NA = 0.9) used to focus the laser beam onto the surface of substrates (with a spot of size ~ 1 μm^2). The estimated laser power at each pixel was 0.16 mW, which is

similar to the power used in literature[59] on similar substrates with negligible photodegradation. Line focus acquisition mode was used and the system was carefully calibrated with a silicon standard (centered at 520 cm^{-1}) to make sure that the laser intensity was uniform at each pixel. Streamline Plus® Raman mapping was conducted on the same area (16 μm × 8 μm, 20 × 10 = 200 spectra for each mapping) for a particular substrate of a given concentration of R6G. Five mappings were acquired sequentially (thus in total 5 × 200 = 1000 spectra for each substrate at a given concentration). This allows for fast Raman measurements without suffering from poor signal-to-noise ratio. By comparing mappings obtained at different times, it is possible to get information on the temporal evolution of the substrates. 15 s exposure time, 1 accumulation and 1200 lines/mm diffraction grating were used. Each mapping took about three minutes to be completed.

The six concentrations used for each substrate range from 0 to 20 μM. All preparation of R6G solutions were performed by diluting the stock solution of 5 mM. For example, the lowest non-zero concentration for Au7 substrate used in the SERS experiment was 0.5 μM, the following procedures were done to realize this: take 200 μL of 5 mM (stock solution) and add 3800 μL pure water to reach 4 mL of 250 μM solution; then take 42 μL from the 250 μM and add 958 μL of pure water to reach 1 mL of 10.5 μM solution; finally add 50 μL of the 10.5 μM solution to a 1 mL pure water (0 M concentration) to reach a final concentration 0.5 μM. All the other solutions with different concentrations were prepared in similar way.

The first experiments were realized with 1 mL of pure water (0 M concentration). After taking five streamline mappings (1000 spectra in total), a pipette was used to add 50 μL R6G 10.5 μM to the solution in the cell to make the final concentration 0.5 μM. Then five more streamline mappings (another 1000 spectra in total) were taken for that concentration. The concentrations were increased like this five times. Thus, for each substrate, 6000 spectra were recorded, 1000 spectra for each concentration.

2.5 Data analysis

2.5.1 Background removal

All the raw spectra were put into an algorithm called COBRA in Matlab. COBRA was developed by Etchegoin et al.[60] specifically to remove the background in SM-SERS situations. This algorithm is based on Wavelet Transform[60], which serves as a very useful tool to process signals with very low frequency events (exactly the types of signals obtained from SM-SERS experiments). COBRA is suitable for situations where thousands of spectra need to be background corrected and the backgrounds vary greatly across the spectra.

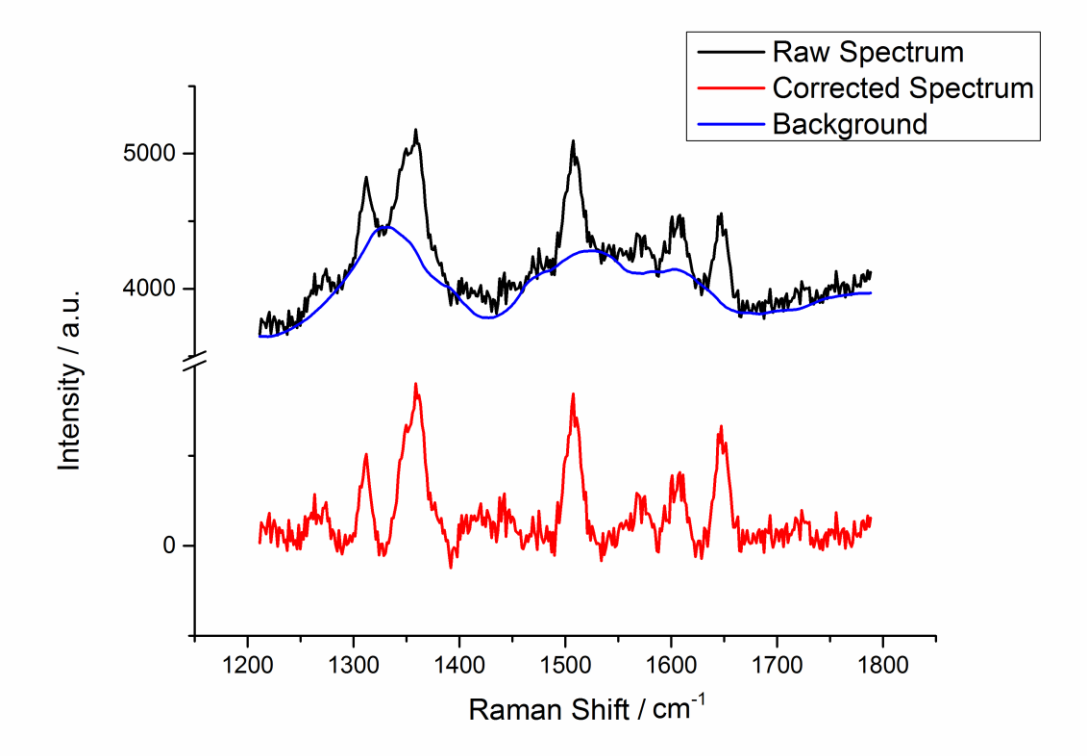

Figure 2.11 Background removal of a typical raw spectrum. The black spectrum is the raw spectrum, the blue line underneath is the background and the red spectrum below is the background corrected spectrum

Figure 2.11 shows the background removal of a typical raw spectrum (The 133th spectrum for Ag3 at 2 μM of R6G solution). The black spectrum is the raw spectrum, the blue line

underneath is the background and the red spectrum below is the background corrected spectrum. The background correction is performed using Wavelet Transform: type: db, 4 level; transform levels: 5; iterations: 10 in COBRA algorithm. It is clear that this set of parameters accurately captures the background and retains most of the Raman features of the raw spectrum. The background removal was performed separately for different concentrations to ensure that different sets of parameters were employed to best capture the backgrounds for different concentrations.

2.5.2 Principal Component Analysis (PCA) introduction

Principal Component Analysis (PCA) is a well-established method that finds applications in all domains of sciences, including botany[61], cosmology[62] and climatology[63]. It has built-in functions to perform linear transformation of the dataset to achieve "dimension reduction". This means that PCA finds the most relevant features that contribute most to the variations of the dataset and discard the rest. It works extremely well when the dataset is mostly the linear combination of independent variables. Detailed description of PCA can be found in the specialized literature[64], here only the most relevant information is provided.

SERS spectra obtained at relatively low concentrations of a certain dye are composed of several contributions, including the very spectrum of the dye and many other variables, such as noise, spectra from contaminations and potential photo-degraded products. PCA is useful in reducing the variables to the one (spectrum from the dye) that contributes most to the dataset (identified as principal component 1, as will be discussed later).

After performing PCA, three major results are obtained: principal components (eigenvectors) of the dataset (and their corresponding explained variation, associated with eigenvalues across the dataset), coefficients and PCA representatives of each spectrum in the dataset.

Principal components (PC) or eigenvectors from the covariance matrix of the dataset, are the variables that account for the variations of the dataset. All the PCs are identified after analyzing

the dataset using PCA. PCs correspond to unique spectral features that exist across the dataset and, in particular, they represent the unique vibrational spectral information provided by the species visiting hot spots during an experiment. In theory, all the PCs can be obtained; however, since only those that contribute most to the dataset (i.e. the spectrum R6G) are required, then only the first few PCs are significant.

After the analysis, every PC is assigned its own eigenvalue, and all the PCs are ordered from the one with the largest eigenvalue to the one with the lowest. This ordering is essentially to put all the PCs in sequence according to the percentage of variation accounted from each one of them. Therefore, the first PC (PC1) accounts for the largest variations in the given dataset and the second PC (PC2) accounts for the second variations etc. In the literature[65], when bi-analyte technique is used in SERS experiments, the first two PCs can explain more than 98% of the variance of the dataset, with each PC corresponding to the spectrum of one dye molecule.

Coefficients represent how much each PC contributes to each spectrum in the dataset. Considering the first two PCs as unit vectors , then each spectrum can be represented by a dot in two-dimension space. When PC1 alone explains almost all (> 95%) of the variation in the dataset, then its coefficients are the only ones that need to be considered. In all SERS experiments in this thesis, only one dye (R6G) was used. In this case, PC1 is the spectrum of R6G, and the coefficients can be taken as the intensities for the spectra (Raman signal). Normally, researchers use the intensity of only one vibrational SERS band to further their analysis, but this procedure takes into account the information from the whole Raman spectrum, rather than focusing on just one band. This is a more precise approach to determine the “intensity” of SERS signals.

The third valuable piece of information is the PCA representations of each spectrum. They are obtained by adding PC1 and PC2, multiplied by their corresponding coefficients. Since PCs that represent features of noise or other unimportant contributions are discarded (only the first two PCs are retained), the PCA representations thus have cleaner background and smoothed lines.

PCA is suitable for the analysis of SERS spectra due to two advantages. As discussed above, PCA is able to extract the most salient features across the dataset. Therefore, the contributions to the SERS spectra from R6G should be extracted as PC1 and the contribution from the rest of variations (noise, possible spectra from photo-degraded products etc) are discarded. Therefore, the first advantage is that the signal-to-noise ratio is improved after PCA treatment. The second advantage is that PCA is able to reject spurious spectra that contaminate the dataset.

In this thesis, the baseline corrected spectra (by COBRA in matlab) were analyzed by PCA using the R 2.7.0 software to improve the signal-to-noise ratio, extract the PC1 (SERS spectrum of R6G) from the dataset, and obtain coefficients for the first principal component, which are used as the intensities of the spectra. The five mappings of the same area for a particular concentration for one substrate are combined (thus 1000 spectra in total) to present histograms for further analysis.

2.5.3 PCA results

As mentioned in 2.5.2 Principal Component Analysis (PCA) introduction, three main results were obtained after PCA analysis. The first is PCs and their corresponding eigenvalues and explained variance. The second is the coefficients for each PC. The third is the PCA representation of all the SERS spectra.

Figure 2.1212 shows the eigenvalues for the PCs obtained after PCA for all the 36,000 spectra (all datasets). It is very clear that PC1 has the largest eigenvalue. The values are close to zero after PC3, which is expected since the later PCs represent just noise.

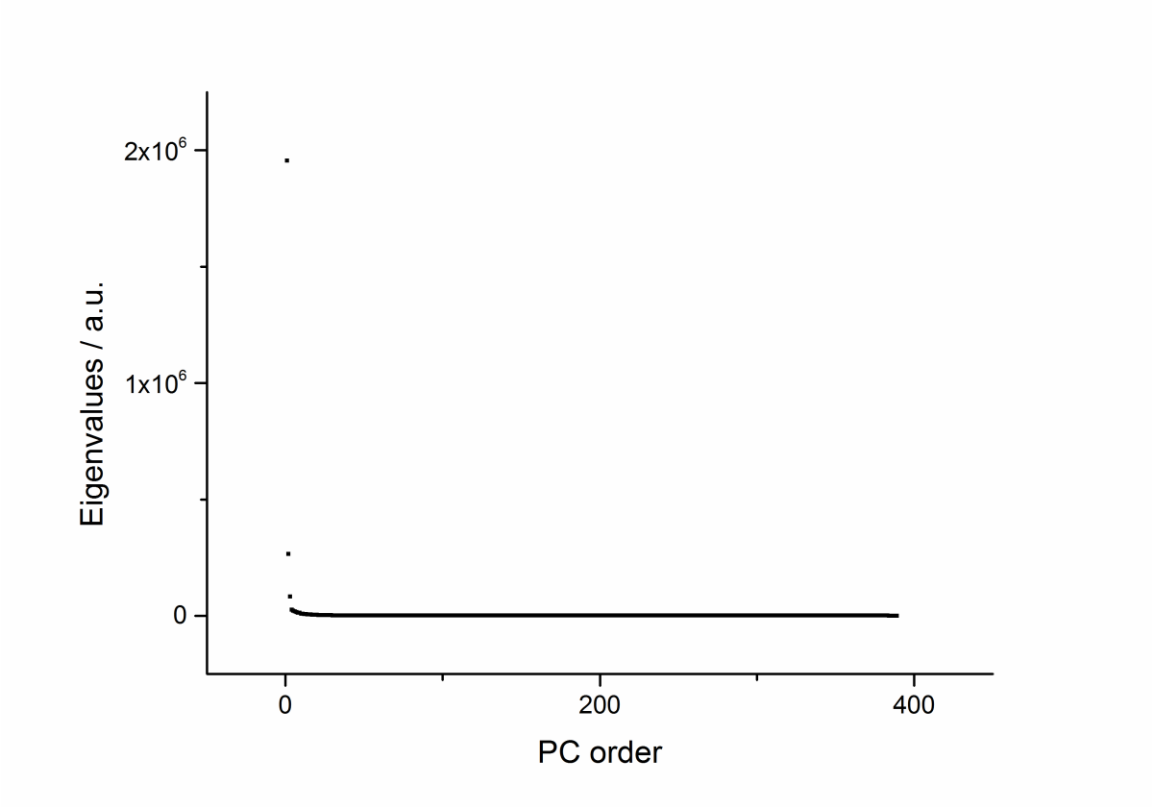

Figure 2.12 Eigenvalues of PCs, representing how much each PC contributes to the overall variation within the dateset

In PCA, the explained variance (EV) can be calculated using the following formula:

$$EV_i = \frac{ev_i^2}{\sum_i ev_i^2} \tag{3.1}$$

where EV_i is the explained variance of the ith eigenvector. The ev_i is the eigenvalue of the ith eigenvector. The explained variance of the first two PCs from Figure 2.1212 can then be calculated. The first PC explains 97.93% of the variance, the second one does 1.81% and the higher order PCs make up only less than 1% of the total variance. This shows that only the first PC from Figure 2.1212 is needed for further analysis.

PC1 is shown in Figure 2.133. It is consistent with all the expected peaks of R6G in the range of 1200 cm^{-1} to 1800 cm^{-1}. This result; therefore, shows that PCA does extract the main

information (in this case, the R6G SERS spectrum) from the dataset, even if an individual spectrum is mixed with noise (See Figure 2.11) and other non-R6G spectral features (resulting from potential photo-bleaching, for instance). The data in Figure 2.133 also confirms that the effect of photo-bleaching and other photo-degradation processes are not prominent (small contributions to the total variation).

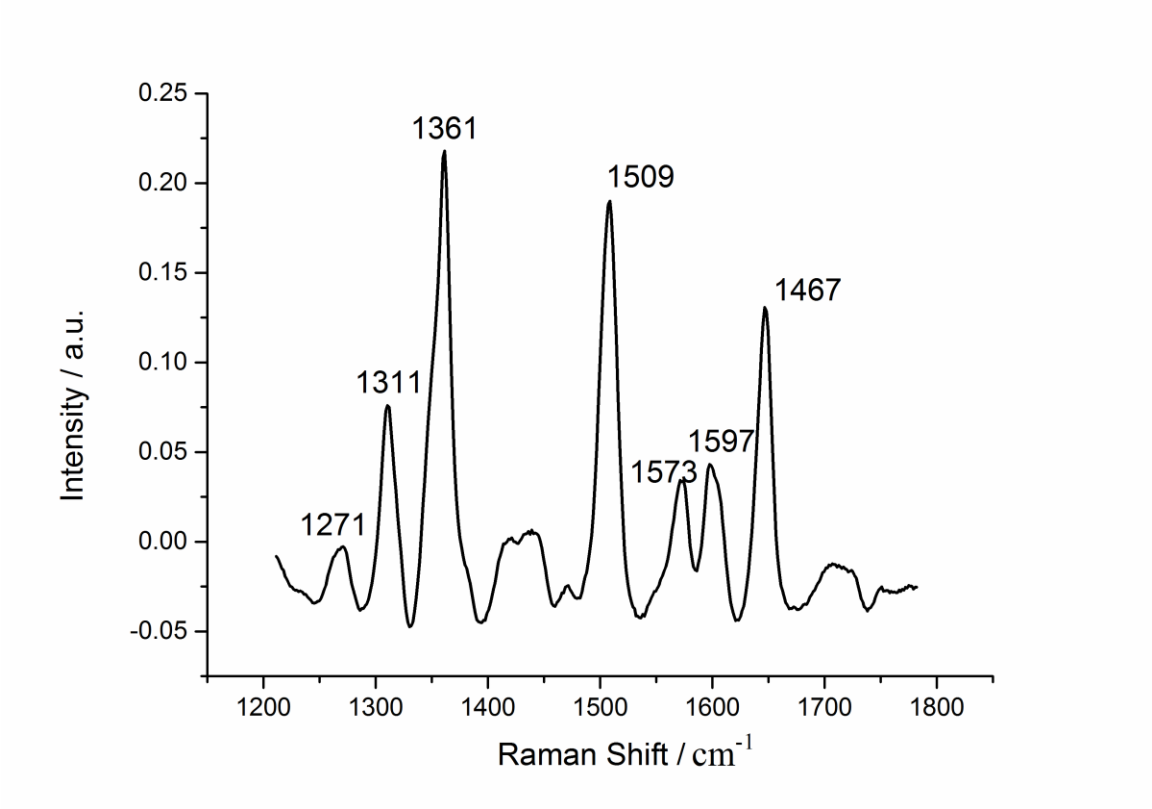

Figure 2.13 First Principal Component (PC1) of Raman spectra

As discussed in 2.5.2 Principal Component Analysis (PCA) introduction, coefficients of PC1 are also obtained from the analysis. However, before proceeding to use these coefficients, one needs to consider the potential for artifacts due to PCA. For instance, if a raw spectrum is a null event, its PCA representation may still have a small contribution of PC1. This is an artifact of performing PCA (trying to fit the fluctuations of the noise) and it can influence the ultimate information (intensity distribution histograms) desired from the data. Figure 2.144 shows a

typical noisy spectrum (black line) and its PCA representation (red line) for Ag3 substrate at 0.4 μM R6G concentration. The spectrum contains considerable noise without any observable, signal but its PCA representation clearly shows small peaks that are misleading. Therefore, those null events must be removed.

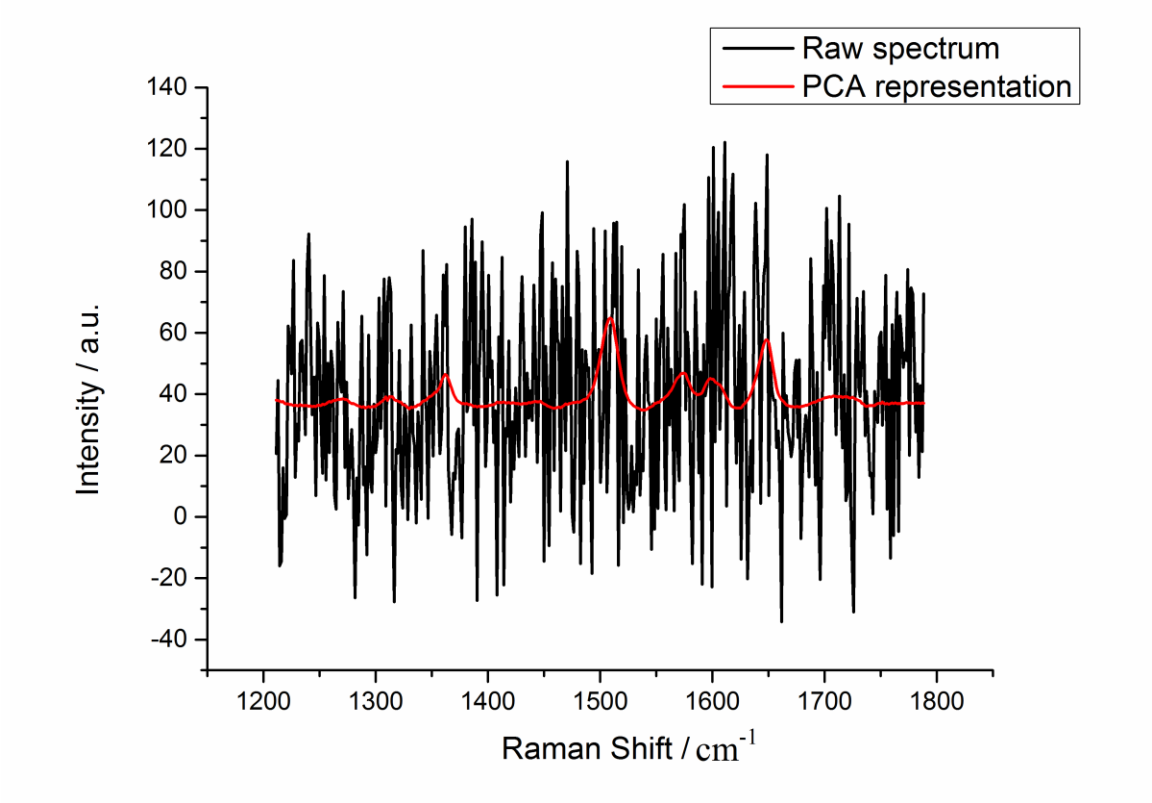

Figure 2.14 One typical noisy spectrum and its PCA representation

This can be achieved by setting a noise cut-off to the dataset. Only events above the cut-off are considered to be non-zero events and retained. The cut-off value could be set according to the standard deviation of error (a null spectrum minus its PCA representation) with respect to the artificial peak intensity. Only peaks with intensities larger than 3 times of the standard deviation are accepted. There are other ways to determine the noise level, but the results should be checked to make sure that the retained spectra are actually not related to null events.

After applying the noise cut-off to the coefficients, one can plot the values of the coefficients against the event number (concentrations) to check the results. Figure 2.155 shows the plot for Au3 substrate. The x-axis in Figure 2.155 represents event number and the first 1000 points correspond to the first concentration (labeled below) used in the experiment, which is 0 μM (water without R6G). The values for the other concentrations are labeled in Figure 2.155. At low concentration (0 μM), no signal is observed (all null events; therefore, all coefficients are 0). SERS signals begin to appear as the concentration increases at 1 μM and there is an increasing trend for higher concentrations.

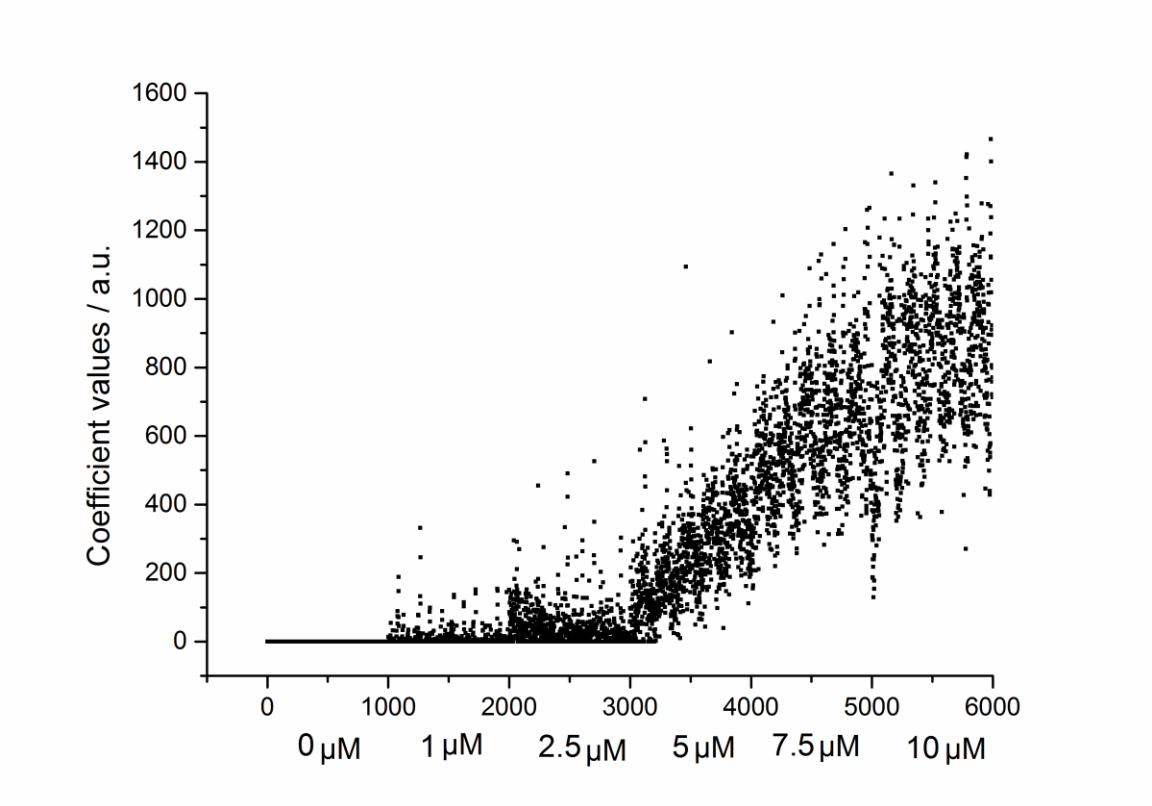

Figure 2.15 Coefficients of PC1 for Au3 substrate against concentrations

2.5.4 Intensity histogram results.

In 1.3.4 Statistics of signals, Monte Carlo simulated intensity histograms against the number of molecules on the surface (hence concentrations if the system is in equilibrium) were shown (Figure 1.3). All substrates in the thesis present similar trend experimentally; i.e., they transition from a long-tail distribution at low concentrations to a Gaussian distribution at higher concentrations. All the histograms were constructed using the Scott method to calculate the bin width[66]:

$$h_n = 3.49sn^{1/3} \tag{3.2}$$

Where s is the standard deviation and n is the number of elements in the dataset.

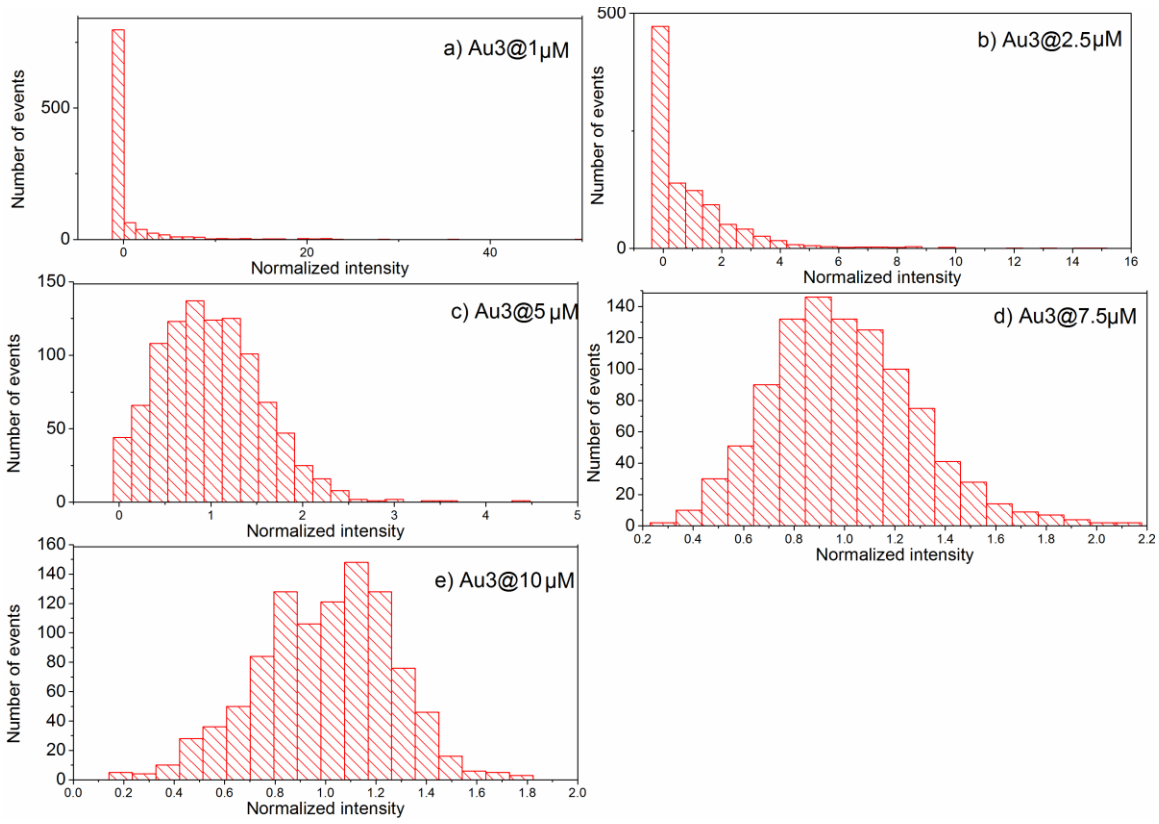

Figure 2.16 Normalized intensity histograms for Au3 substrate measured in the R6G solution of a) 1 μM, b) 2.5 μM, c) 5 μM, d) 7.5 μM and e) 10 μM

Figure 2.166 shows the examples of histograms obtained for the Au3 substrate, after normalizing the coefficients at each concentration to their average. Each count in the histogram is

the coefficient (equivalent to SERS intensity) of one spectrum obtained from mapping (20 × 10 pixels, namely 200 spectra per mapping) the same area (16 μm×8 μm) five times. The histograms were constructed using the coefficients of all of the spectra obtained during the five mappings to improve the statistics.

The results of the lowest concentration (1 μM, Figure 2.166a) show a long-tail distribution in the intensity profile, with a large number of zero events. This indicates that at such a low concentration, Au3 substrate is clearly in the SM regime, where the majority of events are pure noise, but once the molecules find a hot spot, a non-zero event is seen (see 1.3.4 Statistics of signals). The events with intensities around 40 times higher than average correspond to molecules that happen to find the exact hot spot and produced SERS spectra with larger-than-usual intensity. There are a small number of events since the probability for the molecules to find a high enhancing hot spot is low.

Similar shape of intensity histogram was observed for the 2.5 μM concentration (Figure 2.166b). The only differences are that the number of zero events is much smaller than that at 1 μM (Figure 2.166a), and that there are fewer larger-than-usual-intensity events. When the R6G concentration reaches 5 μM (Figure 2.166c), a clear peak emerges in the distribution and there are fewer zero events. The long tale becomes shorter and accordingly the larger-than-usual events reach values only as large as 5 times the average. This is a much smaller value than observed in SM regime (Figure 2.166 a and b). For Au3 substrate at R6G concentrations of 7.5 μM (Figure 2.166d) and 10 μM (Figure 2.166e), a nearly Gaussian distribution is observed with no zero intensity events, which is the characteristics of the average SERS regime.

All the substrates listed in Table 2.1 show the same trend in their intensity histograms as in Figure 2.16. These results agree well with the simulations presented in 1.3.4 Statistics of signals (Figure 1.3).

Chapter 3 Analysis and Discussion

Chapter 2 summarizes the experimental aspects, substrate characterizations and the approach for data analysis. The description was mainly qualitative, focussing on parameters such as surface morphology, obtained by SEM, UV-vis features, and intensity histogram shapes at different concentrations. In this chapter (Chapter 3), a quantitative method to compare SERS substrates, briefly introduced in 1.4 Research Objective, will be presented in length. Before getting into a lengthy mathematical discussion, one question needs to be answered: What does it mean for substrate A to be a better substrate than substrate B? In other words, what properties are required for "a good SERS substrate"?

3.1 What is a good SERS substrate?

We propose two guidelines to determine the quality of a SERS substrate:

1). Good SERS substrates exhibit average-SERS behaviors at low concentrations.

2). Good substrates exhibit less fluctuations in SERS intensities at the same (low) concentrations than bad ones.

The first guideline has been briefly discussed in 1.4 Research Objective. Using the concept of hot spot; i.e., the nanometric region with highly localized electromagnetic field that is able to enhance the Raman signal to a large extend, the concept of an ideal substrate can be revisited: in this case, every spot is highly enhancing and the enhancement is the same across the substrate. If there is only one adsorbed molecule in the whole system, no matter where the molecule adsorbs, approximately the same SERS signal intensity is expected. Small variations may arise from the non-uniformity of the laser illumination, random noise and changes in the orientation of the molecule attached to the surface. When a large number of SERS spectra are taken from this ideal SERS substrate and the intensity histogram is plotted, a Gaussian distribution of intensities with a

sharp peak is expected. This result was categorized as a typical average-SERS behavior (see 1.3.4 Statistics of signals). Since there is only one molecule in the whole SERS system, which is the lowest possible (non-zero) surface concentration, the ideal substrate should exhibit average-SERS behavior (Gaussian distribution) even at the lowest possible concentration.

The opposite situation, namely the worst possible SERS substrate, should provide no noticeable enhancement regardless of the number of molecules on the surface. Even when the surface is saturated (highest molecular concentration), when a large number of SERS spectra are taken from this type of substrate, the intensity histogram will contain only zero intensity events since there is no signal. The large number of zero intensity events is a typical SM behavior, as indicated in 1.3.4 Statistics of signals. Therefore, the worst substrate, even at the highest possible concentration (surface is saturated), will exhibit "SM behavior". The extreme idealized cases described above illustrate the first guideline: good SERS substrates exhibit average-SERS behaviors at low concentrations.

In reality, a perfect SERS substrate does not exist. Fabricated real substrate behaves somewhere along the two extreme cases discussed above. For instance, considering a more realistic substrate with only one hot spot, when there are few molecules on the surface (low concentration). In this case, molecules will be adsorbed outside the hot spot most of the time, resulting in a large number of zero intensity events. However, there is still slim chance that a molecule happen to find the hot spot and, resulting in observable signals. Since the enhancement ability decreases exponentially from the centre of the hot spot to the outside[25a], the observable SERS signal will vary hugely, depending on where exactly the molecules adsorb in the hot spot region. However, because the probability for the molecules to find the most enhancing region of the hot spot is low, the number of high the intensity events will be low and they will appear with an intensity value much larger than the average. This will lead to a long-tailed intensity distribution histogram, with a large number of zero intensity events. This tailed behavior is also a typical "SM signature". At a high concentrations (high surface coverage), there are always

molecules at the hot spot, so signals can be observed in every SERS measurement. Considering the statistical fluctuation and other random errors in the system, a Gaussian distribution is expected for the intensity histogram due to central limit theorem[67].

Now consider another substrate with more than one hot spot: at low concentration, it is still unlikely that molecules will find a hot spot, so a large number of zero intensity events are expected. However, since there is more than one hot spot, the probability to find the hot spots is higher than a substrate with only one hot spot. In this case, more events with non-zero intensities should be observed even though the overall probability is still low. At the high concentration limit, on average, there are always molecules in the hot spot region, leveling out the statistical fluctuation. Therefore, better substrates (in this case one with more hot spots) exhibit less fluctuation (in this case one with only one hot spot) at the same concentration, which is the second guideline.

Again, the two guidelines are:

1). Good SERS substrates exhibit average-SERS behaviors at low concentrations.

2). Good substrates exhibit less fluctuations in SERS intensities at the same concentration than bad ones.

Based on these two guidelines, five criteria were defined to compare SERS substrates:

Better SERS substrates are the ones

A. with higher density of hot spots (density)

B. with highly enhancing hot spots (enhancement)

C. with lower enhancement variations between the hot spots (variation)

D. with higher repeatability (repeatability)

E. that exhibit Gaussian distribution in their intensity histogram at a lower concentration (Shape of the intensity histograms)

The following sections will address each of the five criteria one by one. Please note that all the comparisons are made based on the statistics obtained in the SERS experiments and that the

SERS performance of a substrate can vary depending on the experiment conditions. Therefore, the comparison and the conclusion in this thesis are only relevant to the experiment conditions specified in 2.4 Raman Instrumentation

3.2 Density of hot spots

Ideally, good SERS substrates should have a high density of hot spots. Unfortunately, it is difficult to locate and quantify the exact signal-enhancing region (the size of a hot spot) in real substrates, since the enhancement ability is the highest in the centre of a hot spot and the it decreases exponentially away from the centre[25a] (Figure 1.1). Moreover, the enhancing characteristics of a hot spot (enhancement factor) should also be considered, rather than just counting the number of hot spots on a particular surface area.

However, the problem can be tackled from another perspective. Denser hot spots mean a higher probability for molecules to get adsorbed in Raman-enhancing region, leading to fewer zero-intensity events during mapping. That is to say, when comparing SERS substrates, the one denser in hot spots will have fewer number of zero-intensity events at the same concentration.

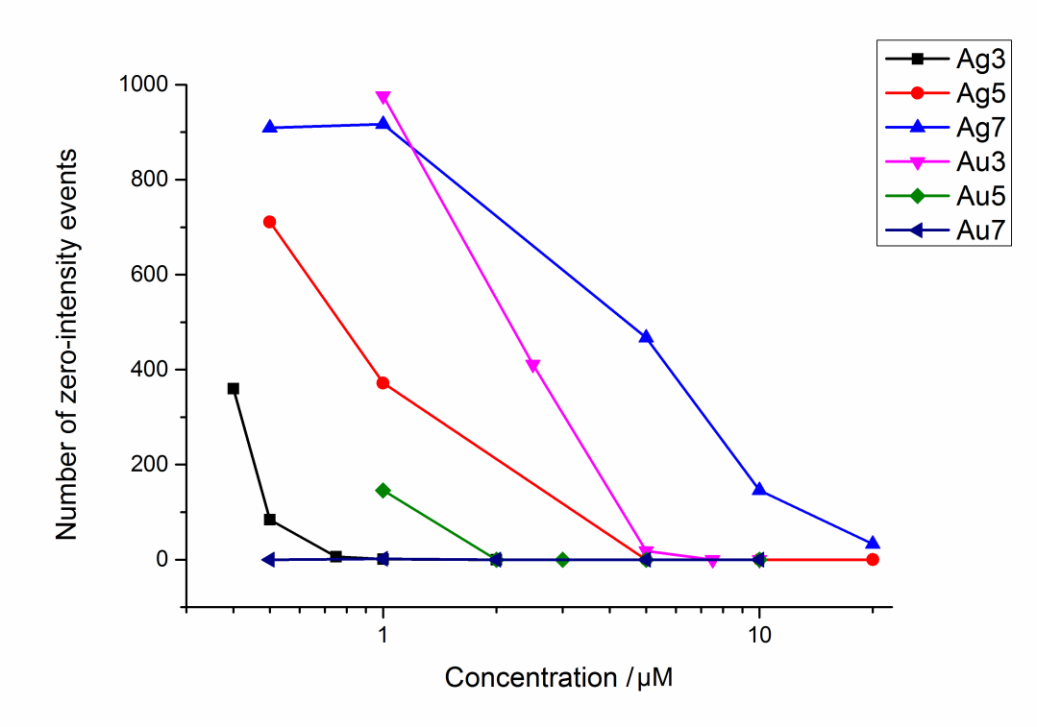

Figure 3.1 Number of zero-intensity events for different substrates against the R6G concentrations (log scale)

Figure 3.1 shows the number of zero-intensity events (in a logarithm scale) obtained from the mappings against the concentration of R6G for different substrates (the substrates were named according to Table 2.1). The total number of events (SERS measurements) for a substrate at a specific concentration was 1000 (see 2.4.3 SERS experiments). When the concentration is below 2 μM, half of the substrates (Ag7, Au3, and Ag5) present more than 500 (half of the total population) zero intensity events. The general trend in Figure 3.1 is that fewer number of zero-intensity events were recorded at higher concentrations. This is because, at higher concentrations, the surface coverage of R6G molecules are higher, leading to a higher probability for a hot spot to be occupied, resulting in fewer number of zero-intensity events, e.g. for all substrates except Ag7, at 10 μM concentration, the numbers of zero-intensity events are all zero.

When all the substrates in Figure 3.1 are compared at the same (low) concentration (1 μM, for instance) in terms of the number of zero-intensity events, the following trend, from the lowest

to the highest, was observed: Ag3>Au7>Au5>Ag5> Ag7>Au3. Note that the actual number of zero intensity events for Ag3 is only one, and for Au7 is two. The difference between them is not statistically significant considering the size of the dataset (1000 spectra in total). Another interesting finding from Figure 3.1 is that, although at 1 μM the number of zero-intensity events for Au3 (976) is slightly larger than for Ag7 (917) , the decreasing trends with the concentration is more pronounced for Au3 than for Ag7. Therefore, the trends in Figure 3.1 indicate that Au3 is a better SERS substrate than Ag7.

Figure 3.1 then indicate that the quality of substrates for SERS, according to the first criterion, follows the order: Ag3≈Au7>Au5>Ag5>Au3>Ag7. The order and the corresponding number of zero-intensity events at 1 μM are summarized in Table 3.1:

Table 3.1 Substrate order and the number of zero-intensity events at 1 μM

Substrate order(from best to worst)	Ag3	Au7	Au5	Ag5	Au3	Ag7
Number of zero-intensity events at 1 μM	1	2	146	372	976	917

3.3 Enhancement of hot spots

It is desired that a good SERS substrate provides large SERS enhancement factors. Therefore having highly enhanced hot spots is another criteria to evaluate a substrate. Quantitatively speaking, the strength of the hot spots can be evaluated by the average SERS intensity, when the experiments are performed in similar conditions (dye concentration and excitation wavelength).

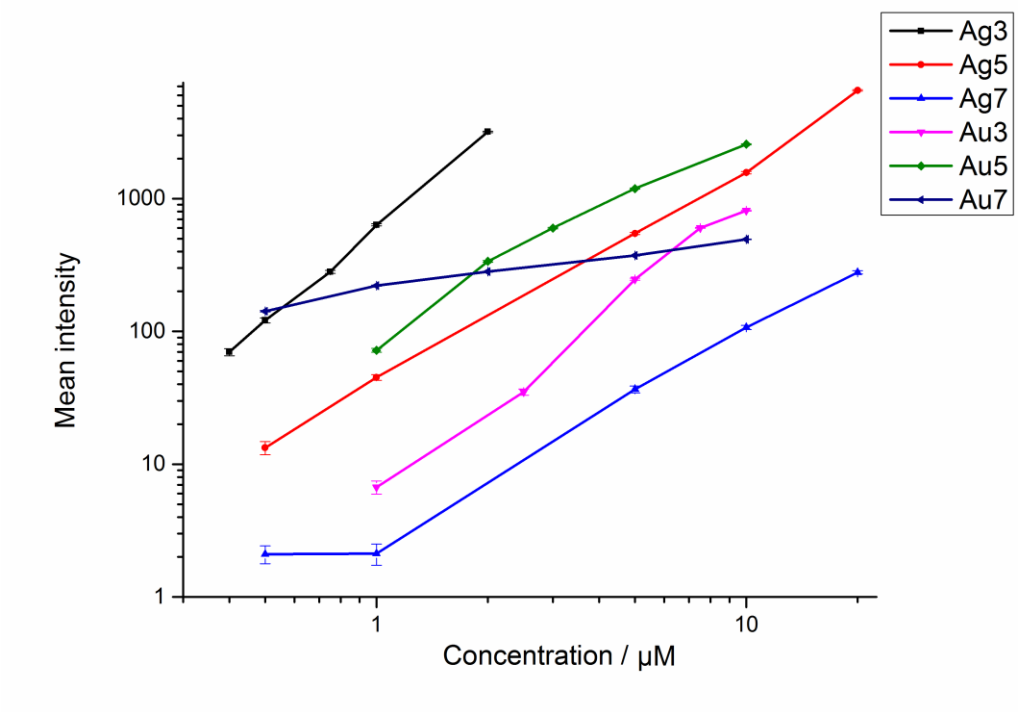

Figure 3.2 Mean intensity against the R6G concentrations (log scale) for different substrates

Figure 3.2 shows the trend of mean intensity versus concentrations for different substrates. The data is presented in a log-log scale. The error bars were calculated using the standard deviation of the intensities at that concentrations, divided by the square root of 1000 (number of data points). The error for each data point is too small to possibly influence the general trend of the intensity increase.

It is very clear in Figure 3.2 that the mean intensity increases with the R6G concentration for every substrate. This is expected, since higher concentration leads to more surface coverage (when the system is in equilibrium) and more molecules contribute to the SERS intensity statistically, resulting in larger average intensities.

It is additionally interesting to find that the trend for all the substrates behaves linearly with a positive slope on the log-log scale. After performing linear line fit to the data points respectively for each substrate (Results are not shown in Figure 3.2), similar slopes were found for all the substrates except Au7 which is obvious from Figure 3.2 that the line for Au7 increased along with

the concentration but the increased amount is less than other substrates. Slopes values are summarized in the Table 3.2

If one compares all the substrates by their mean intensity at 1 μM, then the order from the largest to the lowest is: Ag3>Au7>Au5>Ag5>Au3>Ag7. The order and corresponding mean intensity at 1 μM are also summarized in the Table 3.2. Please note that if the mean intensities at a different concentration are compared, the resultant order might be different due to the much smaller slope of Au7.

Table 3.2 Substrate order and mean intensity at 1 μM

Substrate order(from best to worst)	Ag3	Au7	Au5	Ag5	Au3	Ag7
Slopes values	2.37	0.394	1.52	1.63	2.19	1.64
Mean intensity at 1 μM / a.u.	634	221	71.9	45.0	6.71	2.12

It is also important to note that since the mean intensity for Au7 does not increase at the same pace with others (smaller slopes for Au7), at different concentrations, one may obtain different results for the order. For example, at 10 μM, the order from the largest to the lowest should be: Au5>Ag5>Au3>Au7>Ag7 (missing data points for Ag3), where Au7 becomes the second worst substrate from the second best one at 1 μM. Therefore, if the lines for different substrates intersect, choosing a particular concentration to compare might be arbitrary.

3.4 Variation between hot spots

For an ideal substrate, it is expected that every hot spot on the surface can enhance the SERS signals by the same amount, i.e. SERS enhancement is uniform across the substrate. In reality this is not the case because, as noted in 1.3.2 Hot Spots, the enhancement varies exponentially even in one hot spot on a nanometer scale. In the SERS experiments of mapping, each pixel was on the order of micrometer scale, where there were more than one hot spot in the mapping area.

Therefore, the recorded Raman intensity was the average intensity from the pixel, i.e. the average intensity from more than one hot spot. The variation in this thesis only considers the difference between pixels (micrometer scale).

Better substrates exhibit a more uniform distribution of the enhancement across the surface. Mapping is a good visual tool to qualitatively provide information about the variation. In general, the variation comes from two sources. One is the spatial variation of the enhancement; another one is the SM phenomenon, i.e. variation due to molecules getting in and out of the hot spots. Only the former source corresponds to the quality of the substrates. Therefore, the mapping results in the high concentration need to be used to more accurately reflect the spatial variation, since the surface is saturated and there is little variation due to the movement of molecules and the only source of variation is the heterogeneity of the substrates.

3.4.1 Mapping results

Figure 3.3 mappings was constructed by summing the SERS intensities of individual pixels from the five mappings obtained at R6G concentrations of 10 μM for each substrate (2 μM for Ag3), taking the logarithm of those values, then normalizing them to the range of 0 and 1. The color scale is evenly spaced (note that the red color represents the highest intensity and the black represents zero intensity), and every map is colored using the same scale allowing for direct visual comparison between substrates.

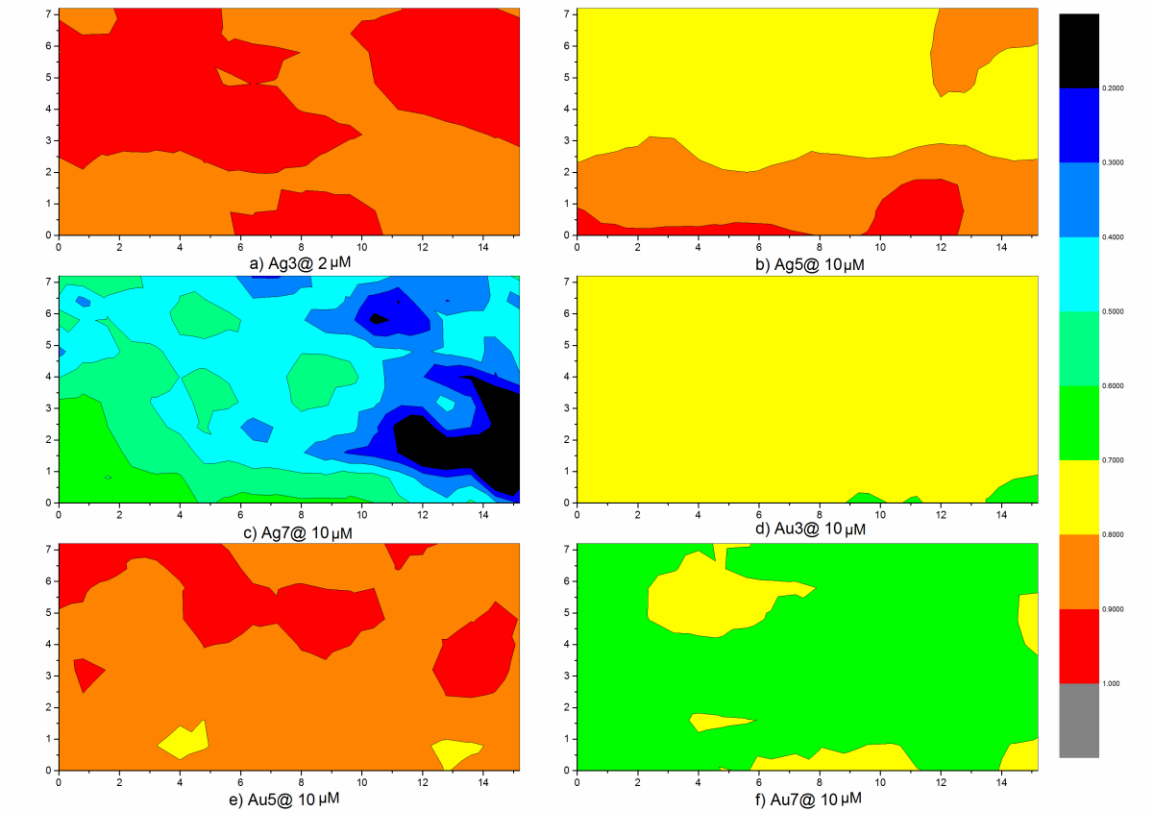

Figure 3.3 Normalized intensity mappings measured in the R6G solution a)of 2 μM for Ag3, of 10 μM for b)Ag5, c)Ag7, d)Au3, e)Au5, and f)Au7. All axes have the unit μm

It is obvious that Figure 3.3a (Ag3) exhibits the largest intensity across the mapping area among all the substrates, although only the dataset from R6G solution of 2 μM is employed here due to the lack of the dataset for Ag3 at 10 μM. Impressions of intensities for other substrates can also be obtained and they correspond well with the data points at 10 μM in Figure 3.2. What is also obviously is that Figure 3.3c (Ag7) has the largest variation across the mapping area due to the large number of different colors (intensities) present and the lowest intensity among all the substrates.

Just by observing the intensity (color) distribution on the mapping area, we can tentatively assume that the spatial variation in the SERS signal is smallest for Ag3, Au7 and Au3, and the largest for Ag7.

3.4.2 Relative standard deviation (RSD)

The relative standard deviation (RSD) of the intensity in the mapping for each concentration can be calculated and indicate the spatial variation. The RSD values were obtained by dividing the standard deviation of the intensities of the 1000 spectra by their mean intensity value. RSD represents how much the individual SERS intensity varies with respect to the mean. Smaller RSD represent less SERS intensity fluctuations, resulting in a better substrate according to this criteria. As mentioned in 1.3.4 Statistics of signals, in the SM regime, the SERS signal exhibits huge fluctuations, since there are only a few molecules on the surface and it is unlikely for them to be adsorbed in a hot spot. In a high concentration regime, the intensity variation across the mapping area more reliably reflects the SERS spatial variation of the substrate. This is because there are molecules everywhere at high concentrations, so that, statistically, during each SERS measurement, the signal at each pixel reflects the quality of the substrate without convolution to the effect of molecules moving in and out of the hot spots, as is the case at low concentrations. Therefore, to evaluate spatial variations of different substrates, the RSD values need to correspond to the average-SERS regime (high concentration for the substrate).

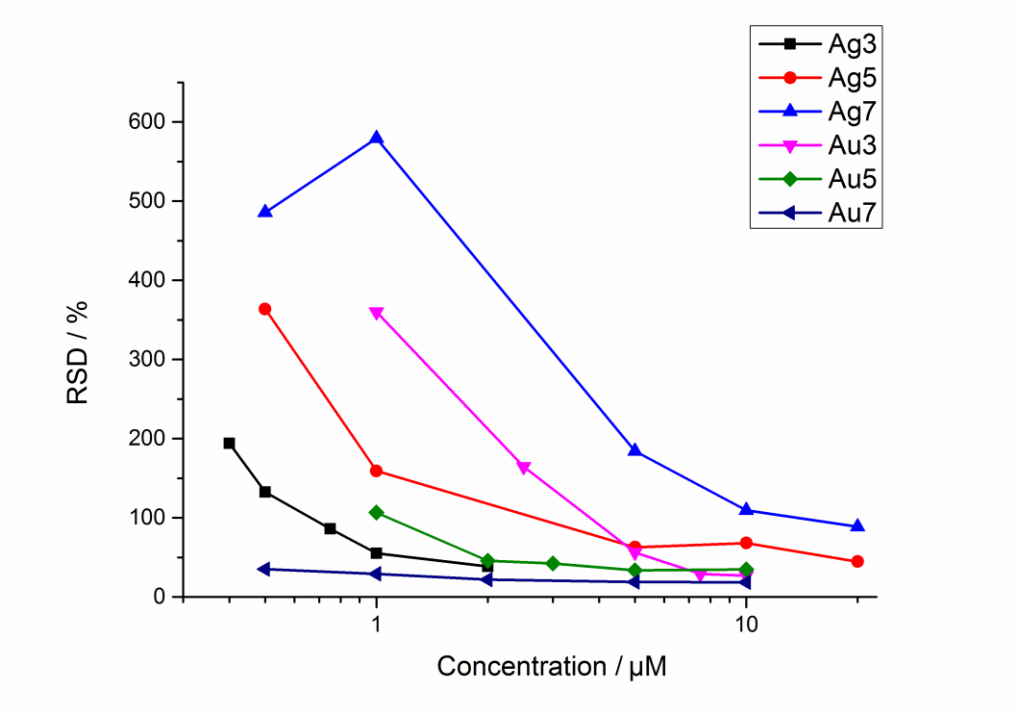

Figure 3.4 RSD against the R6G concentrations (log scale) for different substrates

Figure 3.4 shows how RSD changes for different substrates at each of the concentrations used in the experiments. It is obvious that for each individual substrate, the higher the concentration, the smaller the RSD, resulting in smaller fluctuation. Since RSD values need to be compared at high concentrations, for instance at 10 μM, for each substrate. From the lowest RSD (best substrate in this criterion) to highest RSD (worst one), the following order is obtained: Au7>Au3>Au5>Ag5>Ag7. Note that the data point is missing for Ag3. With its RSD at 2 μM of only 38.7%, which is similar to the RSD (35.0%) for Au5 (color green) at 10 μM, it is possible to estimate that at 10 μM, the RSD for Ag3 will be less than 35.0%. Accordingly, Ag3 should be better than Au5 in this sense.

However, comparing the substrates at 1 μM (data points are available for all the substrates at that concentration), additional insights may be gained in terms of the spatial distribution of SERS intensities. At 1 μM, the ordering from the lowest RSD to largest RSD is: Au7 > Ag3 > Au5 > Ag5>Au3>Ag7. Comparing to the ordering obtained at 10 μm, the relative positions for Au3 and

Au5, Ag5 changes. This shows that some substrates show strong fluctuations of SERS intensities at low concentrations, but the fluctuations decrease quicker as the concentration increases. Also, as mentioned above, at 1 μM, some of the substrates are in the SM regime (this is obvious from the corresponding intensity histograms, for example, Figure 2.16a. However, Au7 and Ag3 substrate exhibits Gaussian-like distribution in their intensity histograms (Results not shown) at 1 μM, indicating both of them are in the high concentration regime at 1 μM, then comparing the RSDs at 1 μM shows that Au7 is better than Ag3 in this criterion.

Taking this information into account provides an insight into where Ag3 might fit. One may tentatively fit Ag3 as better than Au3 but worse than Au7, resulting in the following order: Au7>Ag3>Au3>Au5>Ag5>Ag7, which agrees with the tentative order from 3.4.1 Mapping results. The order and corresponding RSDs at 1 μM and 10 μM are summarized in the Table 3.1

Table 3.3 Substrate order and corresponding RSD at 1 μM and 10 μM

Substrate order(from best to worst)	Au7	Ag3	Au3	Au5	Ag5	Ag7
RSD at 1 μM	29%	55%	360%	106%	159%	579%
RSD at 10 μM	19%	No data	26%	35%	68%	109%

3.5 Repeatability

Spatial variation was discussed and compared for different substrates. Another desired quality for a good substrate is that its SERS results are repeatable, in other words, the substrate has a small temporal variation.

Temporal variation is large at SM regime since the movement of a few molecules on the surface has a significant impact on the SERS signals. However, at higher concentrations, since there are molecules everywhere, there should be no change in the results when repeated mappings are performed (The same argument why results in high concentrations need to be used to

determine the quality of substrates in terms of spatial variation, see 3.4.2 Relative standard deviation (RSD)).

In order to quantity the temporal variation, i.e. repeatability, cross–correlation was use to quantify the similarity among five different mappings in the experiment. The correlation coefficients were calculated in the following way[68]:

$$r = \frac{\sum (x_i - \bar{x})(y_i - \bar{y})}{[\sum (x_i - \bar{x})^2 \sum (y_i - \bar{y})^2]^{1/2}} \tag{3.1}$$

Where x_i and y_i are individual elements of two arrays, and $\bar{x}$ and $\bar{y}$ are corresponding average values for all the elements in each array.

The correlation coefficient is a number between -1 and 1, with 1 being a replica of the two mappings and -1 being exactly negatively correlated and 0 being independent. In this case, because the mappings are highly unlikely to correlate negatively, only positive correlation coefficients are expected. There are five mappings for each concentration, which allows for the calculation of the correlation coefficients between any of the two mappings which can be averaged resulting in a mean correlation coefficient for that concentration.

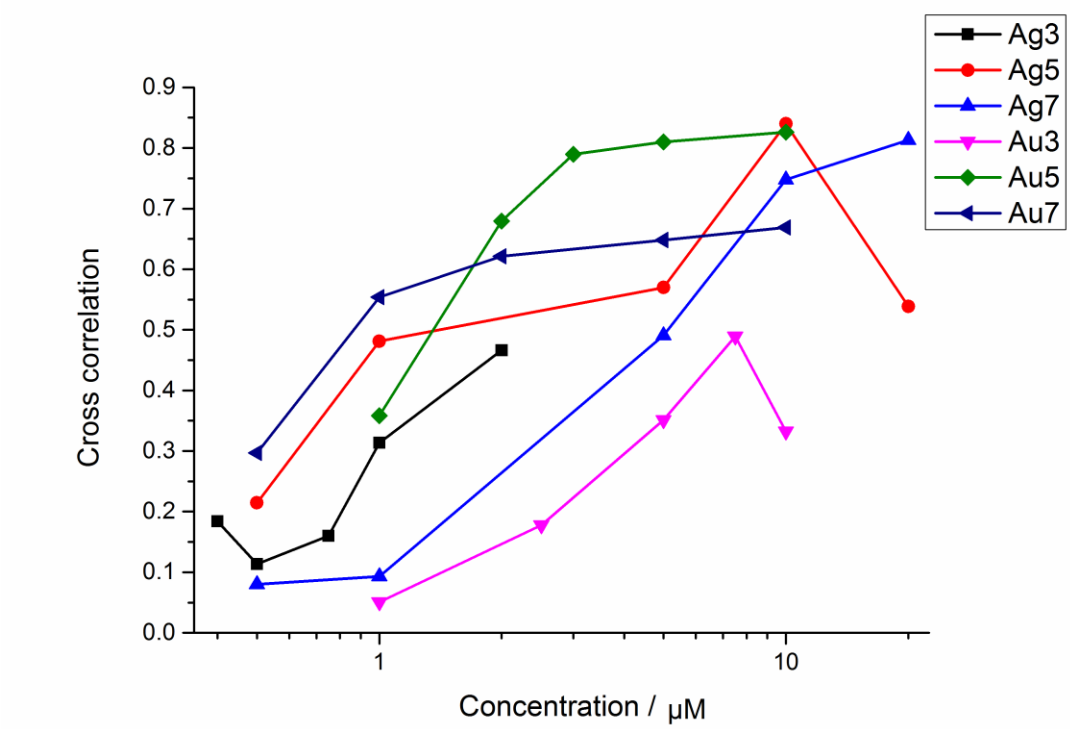

Figure 3.5 Averaged cross correlation coefficients against the R6G concentrations (log scale) for different substrates

Figure 3.5 illustrates the change of average correlation coefficients against R6G concentrations (log scale). It is clear from Figure 3.5 that the average correlation coefficients increase as the concentration increases. At low concentrations, the differences in consecutive mappings arise from a mixture of contributions from the stability of the substrates, spatial distribution of hot spots, and the adsorbing / desorbing processes; resulting in small values of correlation coefficients. As the concentration increases, the molecular processes (adsorption /desorption) has a less impact, resulting in larger values in the coefficients. At high concentrations, the average correlation coefficients reach a value close to 1 and remain constant (saturated) with further increase in the concentration. This is demonstrated by the curves of Au7 (color dark blue) and Au5 (color green); both of which saturate but at different concentrations. Au7 saturates at 1 μM and Au5 does at 3 μM, and their correlation coefficients at saturation were 0.8 for Au7 and

0.65 for Au5. The saturation effect is not clearly visible in Figure 3.5 for all the other four substrates. This may be due to the fact that those substrates were of poor quality, so that even at 10 μM or 20 μM, their mappings still exhibit relatively large temporal variations, suggesting that even higher concentrations (e.g. 50 μM) would be required to observe the saturation. Another interesting finding is that only for Ag5 and Au3 , the curve experiences a drop in its value at the highest concentrations (Figure 3.5). This is counter intuitive since one expects the coefficients to have higher or similar (if saturated) values at a higher concentration. One possible explanation is that the cell on the substrate platform was not totally fixed when the SERS experiment was being performed. If there was a very small vibration on the platform, the cell may move just enough to make a significant change in the mapping area.

By ordering the coefficients at 10 μM (relative high concentrations used in the experiments), from the largest to the lowest, the resultant order is: Ag5>Au5> Ag7 >Au7>Au3. Note that Ag5 (color red, 0.84) and Au5 (color green, 0.83) are very close in their coefficients; therefore comparing their values alone may not reveal the true nature of the substrates. Based on the discussion above, Au5 experiences saturation before 10 μM, but Ag5 does not, so Au5 can be considered better than Ag5. The final order for this criteria is Au5>Ag5>Ag7>Au7>Au3. The order and corresponding correlation coefficients are summarized in 错误！未找到引用源。

Table 3.4 Substrate order and corresponding correlation coefficients at 10 μM

Substrate order(from best to worst)	Au5	Ag5	Ag7	Au7	Au3
Correlation coefficients at 10 μM	0.83	0.84	0.75	0.67	0.33

3.6 Shape of intensity histograms

As stated clearly in 1.3.4 Statistics of signals, the shape of the SERS intensity histograms is concentration dependent. At low concentrations, the histograms present a skewed distribution

with a long tail towards intensities much larger than the average, whereas a Gaussian shape arises at high concentrations. It is suggested that good SERS substrates exhibit a Gaussian distribution in their SERS intensity histograms at lower concentrations (see 3.1 What is a good SERS substrate?).

Two metrics can be employed to characterize the shape of the SERS intensity histograms: skewness and kurtosis.

3.6.1 Skewness

The shape of a distribution can be quantified by way of its symmetry. A long-tail distribution is more asymmetric than a Gaussian-like distribution. In statistics, skewness (*S*) [69] is introduced to describe the symmetry of a distribution. It is calculated in the following way:

$$S = \frac{\frac{1}{n}\sum_{i=1}^{n}(x_i - \bar{x})^3}{[\frac{1}{n}\sum_{i=1}^{n}(x_i - \bar{x})^2]^{3/2}} \tag{3.2}$$

Where the dataset has n data points x_i. $\bar{x}$ is the mean of all the data points. Skewness compares one distribution with a Gaussian (symmetric) distribution. When the value is far from zero (zero is expected for a perfect Gaussian distribution), it means that the distribution is asymmetric. Large values of *S* correspond to more asymmetric distributions. The sign of *S* shows the direction of the skewness: if the value is positive, it means that the distribution is skewed to the left with a long tail on the right (which is exactly the case expected for a SERS system) and vice versa. Therefore, if it is assumed that better substrates exhibit Gaussian distributions (symmetric) of SERS intensity histograms at a lower concentration, it means that their *S*-values should be closer to zero at lower concentrations. In another words, when evaluated at the same concentration, the better substrate will have smaller *S*-values.

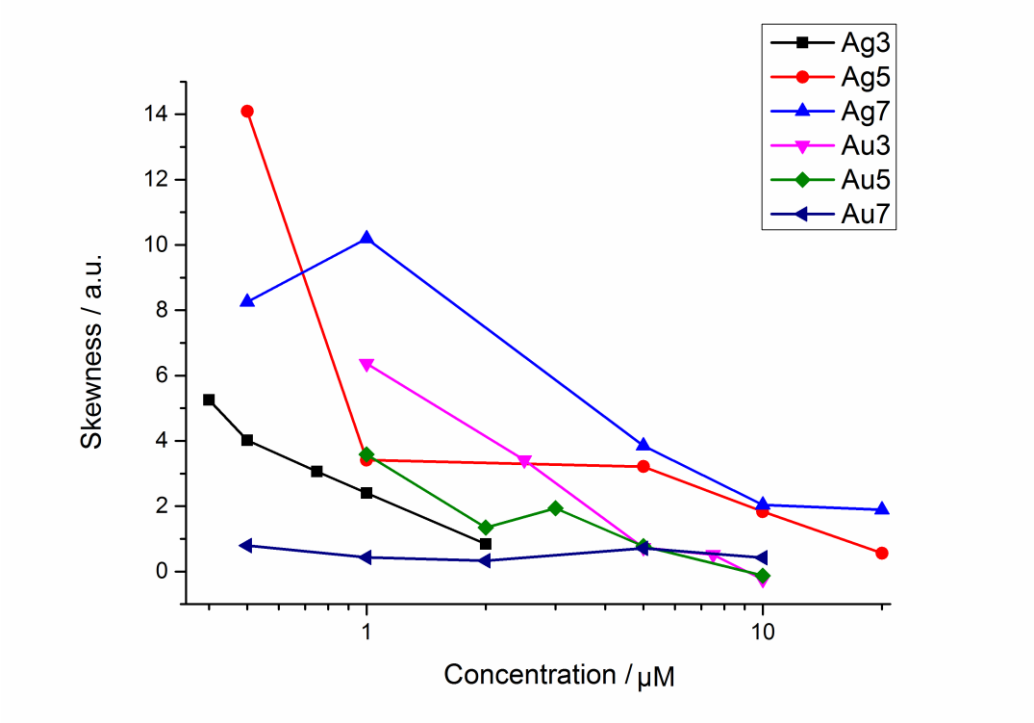

Figure 3.6 *S*-values for different substrates against R6G concentrations (log scale)

Figure 3.6 shows how the convoluted *S*-values against R6G concentrations (log scale) for the different substrates studied in this thesis. The general trend in Figure 3.6 for all the substrates is that the *S*-values decrease as the concentration increases. This trend is expected since all of the substrates exhibit a transition in their distribution shape from a long-tail distribution to a Gaussian curve, i.e. from the asymmetric distribution to the symmetric one, as the concentration increases (see 2.5.4 Intensity histogram results.).

Comparing the skewness values for all the substrates at 1μM the following order (from the lowest (best) to the highest (worst)) is obtained: Au7>Ag3>Ag5>Au5>Au3>Ag7. Note that the values for Au5 and Ag5 are very close. If one looks at the general trend for Au5 (color green) and Ag5 (color red), it is obvious that for most of the concentrations, the values for Au5 are noticeably smaller than those for Ag5, suggesting Au5 is better than Ag5 in terms of skewness.

Allowing for that information when comparing, one can adjust the order to: Au7>Ag3>Au5>Ag5>Au3>Ag7.

However, one thing needs to be addressed before we can finish the discussion on skewness. The simulated intensity histogram results presented in 1.3.4 Statistics of signals are from the same spot on the surface. Therefore, the SERS experiments in this thesis differ in their design than the simulated one. Five mappings of a particular concentrations were performed and the intensities of the total 1000 spectra were used to construct the intensity histograms (see 2.4.3 SERS experiments). In this way, the experiment results are contributed by two factors, the first being the SM phenomenon, i.e. the movement of molecules, that the simulated results are trying to address, and the second being the spatial variation across the mapping area, which is irrelevant in the simulated case. In other words, the spatial variation and the SM phenomenon contribute to the overall shape of the intensity histograms, thus ultimately influencing the quantitative results. In other words, only the contribution from SM phenomenon is needed. Therefore, the results need to be corrected with respect to the spatial variation.

If the mapping results at the highest concentration are considered an accurate indication of the spatial variation, then the following procedures can be performed pixel by pixel to correct the results: normalize the mapping results with the maximum intensity of the highest concentration used for each one substrate; then divide the results of 1 μM by the normalized mapping results of the highest concentration; finally calculate the *S*-values for each substrate at 1 μM. These results are ones without the contribution from the spatial variation.

Both un-corrected and corrected *S*-values at 1 μM for each substrates are summarized in the

Table 3.5. The order changes a bit to Au7>Au5>Ag5>Au3>Ag3>Ag7 with Au7 still the best and Ag7 still the worst. What is obvious is that for all the Au substrates, the *S*-values do not change much after correction while all the Ag substrates exhibit larger *S*-values after correction. This indicates that the removal of the contribution from the spatial variation has a larger impact

on the *S*-values of Ag substrates, therefore, Ag substrates have overall higher spatial variations than Au substrates. This indication corresponds well to 3.4.2 Relative standard deviation (RSD), where in Figure 3.4 at 10 μM, all the Au substrates have less RSD than Ag substrates (missing data point for Ag3) therefore less spatial variation for Au substrates than Ag substrates.

Table 3.5 Substrate order un-corrected and corrected *S*-values at 1 μM for different substrates

Substrate order(from best to worst)	Au7	Au5	Ag5	Au3	Ag3	Ag7
Un-corrected *S*-values at 1 μM	0.43	3.6	3.4	6.4	2.4	10
Corrected *S*-values at 1 μM	0.66	3.0	5.2	5.4	5.5	16.9

3.6.2 Kurtosis

Kurtosis (*K*) is another parameter used to quantify the shape of a histogram. Kurtosis in statistics is used to describe the effect of extreme outliers on a distribution[70]. In other words, *K*-values characterizes "tailedness". It compares the shape of the distribution with a Gaussian distribution. Large *K*-values indicate more departure from Gaussian distribution, i.e. longer tails. Since the SERS intensity histograms transition from a longer tail to a shorter tail (Gaussian-like) as the concentration increases, kurtosis is a good parameter to quantify this transition. Kurtosis is calculated using Equation (3.3):

$$K = \frac{E\{(X-\mu)^4\}}{\sigma^4} = \frac{\frac{1}{n}\sum_{i=1}^{n}(x_i-\bar{x})^4}{[\frac{1}{n}\sum_{i=1}^{n}(x_i-\bar{x})^2]^2} - 3 \qquad (3.3)$$

The *K*-value for a perfect Gaussian distribution is 0. If a distribution has a steeper tail than a Gaussian distribution, its kurtosis value will be smaller than 0; on the other hand, if a distribution

has a longer tail than a Gaussian distribution, its kurtosis will be larger than 0. In SERS experiments, the distributions are more likely to have longer tails than a Gaussian; therefore, *K*-values larger than 0 are expected.

In terms of comparing SERS substrates, the appropriated comparison of *K*-values is for distributions obtained at high concentrations. At high concentrations, all the substrates exhibit more or less a Gaussian distribution in their SERS intensity histograms (see 2.5.4 Intensity histogram results.); thus, kurtosis is a good measurement of how much the larger-than-usual events (tails to the right) influence the overall distribution and no spatial correction is needed as in the case of 3.6.1 Skewness

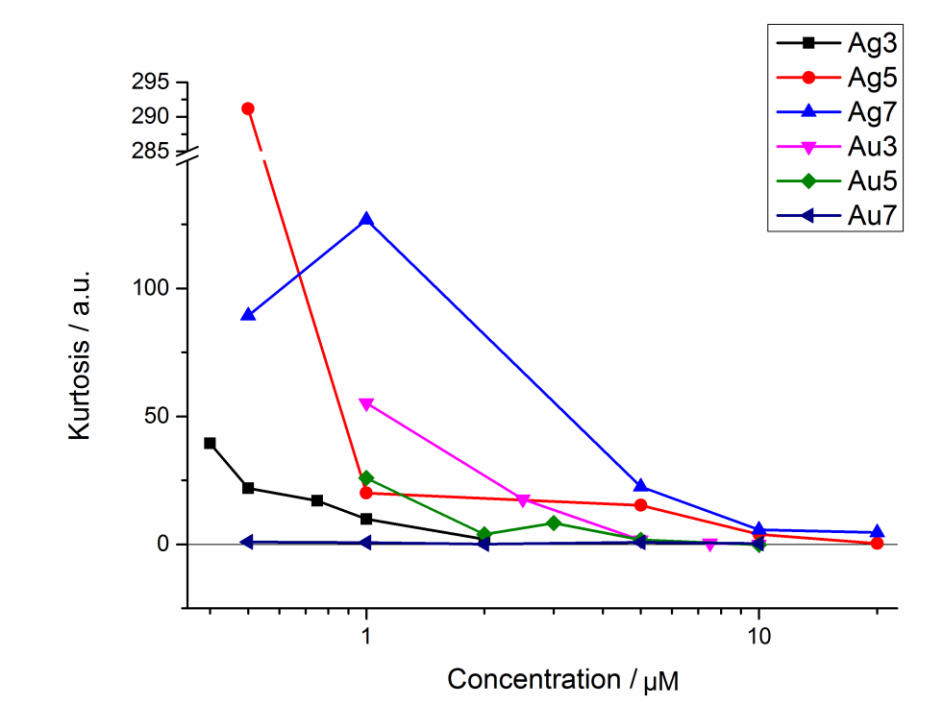

Figure 3.7 *K*-values against the R6G concentration (log scale) for different substrates

Figure 3.7 plots the kurtosis values against the R6G concentration (in a log scale) for all the substrates investigated in this thesis. The general trend in Figure 3.7 is that the kurtosis decreases when the concentration increases. This means that the tail to the right becomes less prominent

(fewer extreme outliers in the distribution) at higher concentrations. It is interesting to note that while all other substrates have kurtosis values that decrease significantly with the increase of concentrations, Au7 (color dark blue) exhibits almost the same kurtosis values (near 0) for all the concentrations used in the experiment. This implies that for Au7, even at 0.5 μM (lowest concentration in the experiment), its fluctuation is limited, which corresponds to the Gaussian-like shape of its intensity histogram at 0.5 μM. It is, therefore, the best substrate among all in terms of this criterion.

Comparing kurtosis values at 10 μM, from the lowest to the highest, the following order is obtained: Au7>Au5>Au3>Ag5>Ag7. The values for Au7, Au5 and Au3 are near 0 and their *K*-values do not tell us much about their qualities. However, tracing the values back to the lower concentrations, the values for Au7 (color dark blue) do not change much, as discussed above; the *K*-values for Au5 (color green) increase slightly and the values for Au3 (color pink) presents a significant increase. Observing the trend for Ag5 and Ag7, the same conclusion as before are found. Therefore, the ordering is validated by both the values at 10 μM and also by the general trend for each substrate. Note that a data point at 10 μM is missing for Ag3 (color black), but by following the trend for Ag3 shows a small number (5.03, smaller than those for all other substrates except Au7) at 2 μM. It is then possible to place Ag3 as the second best substrate, resulting in the ordering: Au7>Ag3>Au5>Au3>Ag5>Ag7. The ordering and kurtosis values at 10 μM are summarized in the Table 3.6

Table 3.6 Substrate order and *K*-values at 10 μM

Substrate order (from best to worst)	**Au7**	**Ag3**	**Au5**	**Au3**	**Ag5**	**Ag7**
K-values at 10 μM	0.3	No data	-0.1	-0.1	6.9	8.6

There is one thing that needs to mention. The simulated intensity histogram results presented in 1.3.4 Statistics of signals are from the same spot on the surface. Therefore, the SERS

experiments in this thesis differ in their design than the simulated one. Five mappings of a particular concentrations were performed and the intensities of the total 1000 spectra were used to construct the intensity histograms (see 2.4.3 SERS experiments). In this way, the experiment results are convoluted by two factors, the first being the SM phenomenon (molecules moving in and out of the hot spots) that the simulated results are trying to address, and the second being the spatial variation across the mapping area that is irrelevant in the simulated case. Therefore, the results of the comparisons above using skewness and kurtosis do not reflect the SM phenomenon directly.

3.7 Summary of the quantification methods

As discussed in the previous sections in this chpater, there are five criteria that characterize different aspects of substrates and there are six metrics (quantifications) of those five criteria to compare different substrates. The results are summarized in Table 3.7.

Table 3.7 Summary of substrate comparisons using different criteria

Substrate criteria	Quantification	Results
1. Density	Number of zero-intensity events	Ag3≈Au7>Au5>Ag5> Au3>Ag7
2. Enhancement	Mean intensity	Ag3>Au7>Au5>Ag5>Au3>Ag7
3. Variation	RSD of intensity;	Au7>Ag3>Au3>Au5>Ag5>Ag7
4. Repeatability	Cross correlation	Au5>Ag5>Ag7>Au7>Au3 (missing data point for Ag3)
5. Histogram shape	Skewness Kurtosis	S: Au7>Au5>Ag5>Au3>Ag3>Ag7 K:Au7>Ag3>Au5>Au3>Ag5>Ag7

Table 3.7 indicates that for different criteria the ordering varies, sometimes in a significant way. For example, in terms of criteria 1, 2, 3 and 5 (Kurtosis), Au7 and Ag3 have the best performances among all and Ag7 has the least, but for criteria 4, Au7 becomes the second worst and Ag7 has somewhat medium performance. Therefore, different substrates exhibit different properties that perform better in certain criteria than others.

However, in light of the majority of the ordering, Au7 and Ag3 can be considered the best substrates. Both share similar surface coverage (density) of hot spots on their surface; Ag3 has higher mean intensity than Au7; in contrast Au7 has less spatial variation than Ag3. Each of these findings paints a picture of how the Au7 and Ag3 differ in their SERS performance. One possible explanation for the difference in behaviors is that Ag3 has "hotter" spots than Au7, meaning that the hot spots on Ag3 are more capable of enhancing SERS signals from the molecules. Despite having highly enhanced hot spots, Ag3 has a larger area of "cold" spots where the signals are not enhanced as much. In contrast, Au7 has a more uniform hot spot distribution but each individual hot spot is not as hot as in Ag3; thus, resulting in less mean intensity, less spatial variation, less fluctuation and more Gaussian-like shape in its intensity histograms. This explanation can be supported by the SEM image of Ag3 and Au7. Figure 2.4 shows the SEM images of Au7 and it is very clear that on a large scale, the triangular nanoparticles are of similar size and are well arranged in the typical laser spot ~ 1 μm^2. It is reasonable to infer that the EM field on the surface is relatively uniform, giving rise to a more uniform intensity distribution under SERS experiments. SEM images of Ag3 are similar to the one shown in Figure 2.5, where defects dominate the whole surface. In a more general sense, the large randomness of Ag3 surface gives rise to unexpectedly large enhancing hot spots, but at the same time, surface roughness is arbitrary and the uniformity is low, resulting in more fluctuation and larger spatial variation. Similar discussions can be undertaken to analyze other substrates.

Another interesting comparison is the size dependent SERS performances for the same material (Au or Ag). For most criteria, Ag3>Ag5>Ag7 and Au7>Au5>Au3. This means that the two materials (Au and Ag) present opposite trends in terms of size. For Ag substrates, NSL technique has been employed to probe into the size effect on the SERS intensity[71]. Wen-Chi Lin et al.[71] investigated SERS signals from Ag nanoparticles arrays using NSL with polystyrene nanospheres of different diameters (430 nm, 600 nm, 740 nm and 820 nm). These experimental parameters were similar to what was used in this thesis (see 2.1.2 Substrates Used In This Thesis). After the SERS experiments, they correlated the Raman intensity (calculated EF) at 10 μM R6G solution with the diameters of the nanospheres (hence the size of triangular nanoparticles on the substrates). Their results do reveal the negative correlation between nanoparticle sizes and Raman intensity. They argue that when the size of Ag nanoparticles increases, the average SERS intensity decreases due to weaker LSPR coupling between Ag particles, leading to smaller EM field near the surface. Furthermore, since the surface area around the nanoparticles are responsible for the enhanced Raman intensity, fewer molecules will be adsorbed onto the surface when Ag particles are larger, leading to weaker Raman intensity. Therefore the resultant order Ag3>Ag5>Ag7 agrees with the previous studies experimentally.

The EM fields around a single triangular nanoparticles have also been investigated by Van Duyne et al.[72], who varied in particle size in the calculation. Similar to the Figure 2.2, they found that the EM field distributions are similar in both cases but the smaller nanoparticle reveals more intense EM field around the tip of the nanoparticle surface. This agrees with our observations that show higher enhanced the Raman signal for smaller the particles. Since local EM fields contribute directly to the signal enhancement (Equation 1.3), the resultant order Ag3>Ag5>Ag7 agrees with the previous theoretical studies l.

However, there are few studies in the literature that focus on the size-dependent SERS intensity for Au substrates derived by NSL method, either experimentally or theoretically. In one study[73], Au nanoframes are fabricated using the Langmuir-Blodgett technique. The more inter-

particle spacing, the more enhancement is observed in the Raman. They attributed this result to the competition between inter- and intra-particle fields in the system. This study implies that Au nanoparticles may behave different in terms of the impact on SERS performance with the change of size from Ag substrates. The resultant order of Au7>Au5>Au3 complies with that study.

It seems that the random surface roughness (Ag3) outperforms other well-arranged substrates for Ag while the reverse is true for Au. Since Au and Ag have very similar coupling effect due to their similar dielectric properties for LSPR[55], it is not obvious why Au and Ag behave in opposite ways. It is possible that random surface defects on the mapping area can contribute to the behavior, so it would be more illuminating if exact surface morphology (SEM image) was correlated with the illuminated area by the laser and if the near-field EM field distributions around nanoparticles are available in the literature.

Chapter 4 Conclusion

To conclude, six different substrates of Ag or Au nanoparticles of different sizes were fabricated by NSL SEM images showed that the substrates with larger nanoparticle sizes (Au5, Ag5, Au7 and Ag7) had a relatively uniform well-arranged pattern of nanoparticles; while substrates with small nanoparticles did not show a clear pattern due to the presence of defects over a large area.

Their SERS spectra were recorded by performing mappings of different concentrations of each individual substrate. Through subsequent baseline correction and PCA, the "intensity" of individual spectrum is represented by its coefficient value of PC1. The intensity histograms of each substrate showed a similar trend as the literature[25a] when the concentration increases.

Instead of adopting the traditional way of comparing different substrates, namely calculating and comparing EF values, five criteria (six quantification methods in total) were employed to comprehensively evaluate the six substrates. These were density of hot spots (characterized by the number of zero-intensity events), enhancement (represented by mean intensity), variation (calculated by RSD of intensity), repeatability (realized by cross correlation) and histogram shape (quantified by skewness and kurtosis).

These new methods provide insight to understanding the properties of substrates in terms of hot spots. First, different substrates may exhibit better performance in terms of one criterion but worse in terms of others. For example, Au7 had the top quality in terms of small enhancement variation and Gaussian-like shape in its intensity histograms at low concentrations, but it did not perform well in terms of repeatability. Second, Au7 and Ag3 among others stood out in terms of their overall SERS performance and interestingly, Ag3 had more averaged intensity than Au7 but had more variation than Au7. This could be explained by the fact that randomly distributed nanoparticles on the surface of Ag3 could potentially form highly enhancing hot spots with more

variations across the mapping area while Au7 had a more uniform distribution of nanoparticles which made the variation smaller but the hot spots less enhancing. The overall performance for Au substrates is Au7>Au5>Au3 and for Ag substrates is Ag3>Ag5>Ag7.

These more elaborated methods are believed to provide a more comprehensive approach to evaluate and compare substrates than the traditional EF values. The thesis also paves the way for future study on SM-SERS and fabricating ideal SERS substrates.

Bibliography

1. Smekal, A., Zur Quantentheorie der Dispersion. *Naturwissenschaften* **1923,** *11* (43), 873-875.

2. Raman, C. V.; Krishnan, K. S., A new type of secondary radiation. *Nature* **1928,** *121*, 501-502.

3. (a) Wang, G. X.; Yang, J.; Park, J.; Gou, X. L.; Wang, B.; Liu, H.; Yao, J., Facile synthesis and characterization of graphene nanosheets. *Journal of Physical Chemistry C* **2008,** *112* (22), 8192-8195; (b) Hernandez, Y.; Nicolosi, V.; Lotya, M.; Blighe, F. M.; Sun, Z. Y.; De, S.; McGovern, I. T.; Holland, B.; Byrne, M.; Gun'ko, Y. K.; Boland, J. J.; Niraj, P.; Duesberg, G.; Krishnamurthy, S.; Goodhue, R.; Hutchison, J.; Scardaci, V.; Ferrari, A. C.; Coleman, J. N., High-yield production of graphene by liquid-phase exfoliation of graphite. *Nature Nanotechnology* **2008,** *3* (9), 563-568; (c) Stankovich, S.; Dikin, D. A.; Piner, R. D.; Kohlhaas, K. A.; Kleinhammes, A.; Jia, Y.; Wu, Y.; Nguyen, S. T.; Ruoff, R. S., Synthesis of graphene-based nanosheets via chemical reduction of exfoliated graphite oxide. *Carbon* **2007,** *45* (7), 1558-1565.

4. (a) Mohiuddin, T. M. G.; Lombardo, A.; Nair, R. R.; Bonetti, A.; Savini, G.; Jalil, R.; Bonini, N.; Basko, D. M.; Galiotis, C.; Marzari, N.; Novoselov, K. S.; Geim, A. K.; Ferrari, A. C., Uniaxial strain in graphene by Raman spectroscopy: G peak splitting, Gruneisen parameters, and sample orientation. *Physical Review B* **2009,** *79* (20); (b) Gupta, A.; Chen, G.; Joshi, P.; Tadigadapa, S.; Eklund, P. C., Raman scattering from high-frequency phonons in supported n-graphene layer films. *Nano Letters* **2006,** *6* (12), 2667-2673; (c) Nordlander, P.; Oubre, C.; Prodan, E.; Li, K.; Stockman, M. I., Plasmon hybridizaton in nanoparticle dimers. *Nano Letters* **2004,** *4* (5), 899-903.

5. (a) Srikar, V. T.; Spearing, S. M., A critical review of microscale mechanical testing methods used in the design of microelectromechanical systems. *Experimental Mechanics* **2003,** *43* (3), 238-247; (b) Georgiev, D. G.; Boolchand, P.; Jackson, K. A., Intrinsic nanoscale phase separation of bulk As2S3 glass. *Philosophical Magazine* **2003,** *83* (25), 2941-2953; (c) Boolchand, P.; Bresser, W. J., The structural origin of broken chemical order in GeSe2. *Philosophical Magazine B-Physics of Condensed Matter Statistical Mechanics Electronic Optical and Magnetic Properties* **2000,** *80* (10), 1757-1772.

6. (a) Kircher, M. F.; de la Zerda, A.; Jokerst, J. V.; Zavaleta, C. L.; Kempen, P. J.; Mittra, E.; Pitter, K.; Huang, R. M.; Campos, C.; Habte, F.; Sinclair, R.; Brennan, C. W.; Mellinghoff, I. K.; Holland, E. C.; Gambhir, S. S., A brain tumor molecular imaging strategy using a new triple-modality MRI-photoacoustic-Raman nanoparticle. *Nature Medicine* **2012,** *18* (5), 829-U235; (b) Kazanci, M.; Roschger, P.; Paschalis, E. P.; Klaushofer, K.; Fratzl, P., Bone osteonal tissues by Raman spectral mapping:

Orientation-composition. *Journal of Structural Biology* **2006,** *156* (3), 489-496; (c) Jones, M. R.; Heerdawson, M.; Mattioli, T. A.; Hunter, C. N.; Robert, B., SITE-SPECIFIC MUTAGENESIS OF THE REACTION-CENTER FROM RHODOBACTER-SPHAEROIDES STUDIED BY FOURIER-TRANSFORM RAMAN-SPECTROSCOPY - MUTATIONS AT TYROSINE M210 DO NOT AFFECT THE ELECTRONIC-STRUCTURE OF THE PRIMARY DONOR. *Febs Letters* **1994,** *339* (1-2), 18-24.

7. (a) Su, F. B.; Poh, C. K.; Chen, J. S.; Xu, G. W.; Wang, D.; Li, Q.; Lin, J. Y.; Lou, X. W., Nitrogen-containing microporous carbon nanospheres with improved capacitive properties. *Energy & Environmental Science* **2011,** *4* (3), 717-724; (b) Yu, Y.; Yu, J. C.; Yu, J. G.; Kwok, Y. C.; Che, Y. K.; Zhao, J. C.; Ding, L.; Ge, W. K.; Wong, P. K., Enhancement of photocatalytic activity of mesoporous TiO2 by using carbon nanotubes. *Applied Catalysis a-General* **2005,** *289* (2), 186-196; (c) Wilson, K.; Lee, A. F.; Macquarrie, D. J.; Clark, J. H., Structure and reactivity of sol-gel sulphonic acid silicas. *Applied Catalysis a-General* **2002,** *228* (1-2), 127-133.

8. Willets, K. A.; Van Duyne, R. P., Localized surface plasmon resonance spectroscopy and sensing. In *Annual Review of Physical Chemistry*, Annual Reviews: Palo Alto, 2007; Vol. 58, pp 267-297.

9. Dresselhaus, M. S.; Dresselhaus, G.; Saito, R.; Jorio, A., Raman spectroscopy of carbon nanotubes. *Physics Reports-Review Section of Physics Letters* **2005,** *409* (2), 47-99.

10. Fleischmann, M.; Hendra, P. J.; McQuilla.Aj, RAMAN-SPECTRA OF PYRIDINE ADSORBED AT A SILVER ELECTRODE. *Chemical Physics Letters* **1974,** *26* (2), 163-166.

11. Albrecht, M. G.; Creighton, J. A., ANOMALOUSLY INTENSE RAMAN-SPECTRA OF PYRIDINE AT A SILVER ELECTRODE. *Journal of the American Chemical Society* **1977,** *99* (15), 5215-5217.

12. Jeanmaire, D. L.; Vanduyne, R. P., SURFACE RAMAN SPECTROELECTROCHEMISTRY .1. HETEROCYCLIC, AROMATIC, AND ALIPHATIC-AMINES ADSORBED ON ANODIZED SILVER ELECTRODE. *Journal of Electroanalytical Chemistry* **1977,** *84* (1), 1-20.

13. (a) Yamamoto, Y. S.; Ishikawa, M.; Ozaki, Y.; Itoh, T., Fundamental studies on enhancement and blinking mechanism of surface-enhanced Raman scattering (SERS) and basic applications of SERS biological sensing. *Frontiers of Physics* **2014,** *9* (1), 31-46; (b) Chowdhury, J., How the Charge Transfer (CT) Contributions Influence the SERS Spectra

of Molecules? A Retrospective from the View of Albrecht's "A" and Herzberg-Teller Contributions. *Applied Spectroscopy Reviews* **2015,** *50* (3), 240-260.

14. Eric C. Le Ru, P. G. E., Principles of surface-enhanced Raman spectroscopy : and related plasmonic effects. 1st ed ed.; Elsevier: Amsterdam ; Boston, 2009.

15. Wang, X. T.; Shi, W. S.; She, G. W.; Mu, L. X., Surface-Enhanced Raman Scattering (SERS) on transition metal and semiconductor nanostructures. *Physical Chemistry Chemical Physics* **2012,** *14* (17), 5891-5901.

16. (a) Zou, S. Z.; Weaver, M. J., Surface-enhanced Raman scattering an uniform transition metal films: Toward a versatile adsorbate vibrational strategy for solid-nonvacuum interfaces? *Analytical Chemistry* **1998,** *70* (11), 2387-2395; (b) Tian, Z. Q.; Ren, B.; Wu, D. Y., Surface-enhanced Raman scattering: From noble to transition metals and from rough surfaces to ordered nanostructures. *Journal of Physical Chemistry B* **2002,** *106* (37), 9463-9483; (c) Tian, Z. Q.; Ren, B.; Li, J. F.; Yang, Z. L., Expanding generality of surface-enhanced Raman spectroscopy with borrowing SERS activity strategy. *Chemical Communications* **2007,** (34), 3514-3534.

17. Lana-Villarreal, T.; Perez, J. M.; Gomez, R., Adsorption studies on titanium dioxide by means of Raman spectroscopy. *Comptes Rendus Chimie* **2006,** *9* (5-6), 806-816.

18. (a) Tao, A.; Kim, F.; Hess, C.; Goldberger, J.; He, R. R.; Sun, Y. G.; Xia, Y. N.; Yang, P. D., Langmuir-Blodgett silver nanowire monolayers for molecular sensing using surface-enhanced Raman spectroscopy. *Nano Letters* **2003,** *3* (9), 1229-1233; (b) Haes, A. J.; Haynes, C. L.; McFarland, A. D.; Schatz, G. C.; Van Duyne, R. R.; Zou, S. L., Plasmonic materials for surface-enhanced sensing and spectroscopy. *Mrs Bulletin* **2005,** *30* (5), 368-375; (c) Anker, J. N.; Hall, W. P.; Lyandres, O.; Shah, N. C.; Zhao, J.; Van Duyne, R. P., Biosensing with plasmonic nanosensors. *Nature Materials* **2008,** *7* (6), 442-453.

19. (a) Lu, Y.; Liu, G. L.; Lee, L. P., High-density silver nanoparticle film with temperature-controllable interparticle spacing for a tunable surface enhanced Raman scattering substrate. *Nano Letters* **2005,** *5* (1), 5-9; (b) Talley, C. E.; Jackson, J. B.; Oubre, C.; Grady, N. K.; Hollars, C. W.; Lane, S. M.; Huser, T. R.; Nordlander, P.; Halas, N. J., Surface-enhanced Raman scattering from individual Au nanoparticles and nanoparticle dimer substrates. *Nano Letters* **2005,** *5* (8), 1569-1574.

20. (a) Hildebrandt, P.; Murgida, D. H., Electron transfer dynamics of cytochrome c bound to self-assembled monolayers on silver electrodes. *Bioelectrochemistry* **2002,** *55*

(1-2), 139-143; (b) Feng, S. Y.; Pan, J. J.; Wu, Y. A.; Lin, D.; Chen, Y. P.; Xi, G. Q.; Lin, J. Q.; Chen, R., Study on gastric cancer blood plasma based on surface-enhanced Raman spectroscopy combined with multivariate analysis. *Science China-Life Sciences* **2011,** *54* (9), 828-834; (c) Wang, Y. L.; Irudayaraj, J., Surface-enhanced Raman spectroscopy at single-molecule scale and its implications in biology. *Philosophical Transactions of the Royal Society B-Biological Sciences* **2013,** *368* (1611).

21. (a) Carron, K.; Peitersen, L.; Lewis, M., OCTADECYLTHIOL-MODIFIED SURFACE-ENHANCED RAMAN-SPECTROSCOPY SUBSTRATES - A NEW METHOD FOR THE DETECTION OF AROMATIC-COMPOUNDS. *Environmental Science & Technology* **1992,** *26* (10), 1950-1954; (b) Rule, K. L.; Vikesland, P. J., Surface-Enhanced Resonance Raman Spectroscopy for the Rapid Detection of Cryptosporidium parvum and Giardia lamblia. *Environmental Science & Technology* **2009,** *43* (4), 1147-1152; (c) Halvorson, R. A.; Vikesland, P. J., Surface-Enhanced Raman Spectroscopy (SERS) for Environmental Analyses. *Environmental Science & Technology* **2010,** *44* (20), 7749-7755.

22. Asiala, S. M.; Schultz, Z. D., Characterization of hotspots in a highly enhancing SERS substrate. *Analyst* **2011,** *136* (21), 4472-4479.

23. Nie, S. M.; Emery, S. R., Probing single molecules and single nanoparticles by surface-enhanced Raman scattering. *Science* **1997,** *275* (5303), 1102-1106.

24. Kneipp, K.; Wang, Y.; Kneipp, H.; Perelman, L. T.; Itzkan, I.; Dasari, R.; Feld, M. S., Single molecule detection using surface-enhanced Raman scattering (SERS). *Physical Review Letters* **1997,** *78* (9), 1667-1670.

25. (a) Le Ru, E. C.; Etchegoin, P. G.; Meyer, M., Enhancement factor distribution around a single surface-enhanced Raman scattering hot spot and its relation to single molecule detection. *Journal of Chemical Physics* **2006,** *125* (20); (b) Etchegoin, P. G.; Meyer, M.; Le Ru, E. C., Statistics of single molecule SERS signals: is there a Poisson distribution of intensities? *Physical Chemistry Chemical Physics* **2007,** *9* (23), 3006-3010.

26. (a) Dieringer, J. A.; Lettan, R. B.; Scheidt, K. A.; Van Duyne, R. P., A frequency domain existence proof of single-molecule surface-enhanced Raman Spectroscopy. *Journal of the American Chemical Society* **2007,** *129* (51), 16249-16256; (b) Doering, W. E.; Nie, S. M., Single-molecule and single-nanoparticle SERS: Examining the roles of surface active sites and chemical enhancement. *Journal of Physical Chemistry B* **2002,** *106* (2), 311-317.

27. Le Ru, E. C.; Blackie, E.; Meyer, M.; Etchegoin, P. G., Surface enhanced Raman scattering enhancement factors: a comprehensive study. *Journal of Physical Chemistry C* **2007,** *111* (37), 13794-13803.

28. (a) Livingstone, R.; Zhou, X. C.; Tamargo, M. C.; Lombardi, J. R.; Quagliano, L. C.; Jean-Mary, F., Surface Enhanced Raman Spectroscopy of Pyridine on CdSe/ZnBeSe Quantum Dots Crown by Molecular Beam Epitaxy. *Journal of Physical Chemistry C* **2010,** *114* (41), 17460-17464; (b) Liu, R.; Liu, J. F.; Zhou, X. X.; Sun, M. T.; Jiang, G. B., Fabrication of a Au Nanoporous Film by Self-Organization of Networked Ultrathin Nanowires and Its Application as a Surface-Enhanced Raman Scattering Substrate for Single-Molecule Detection. *Analytical Chemistry* **2011,** *83* (23), 9131-9137; (c) Steuwe, C.; Kaminski, C. F.; Baumberg, J. J.; Mahajan, S., Surface Enhanced Coherent Anti-Stokes Raman Scattering on Nanostructured Gold Surfaces. *Nano Letters* **2011,** *11* (12), 5339-5343.

29. Le Ru, E. C.; Etchegoin, P. G., Sub-wavelength localization of hot-spots in SERS. *Chemical Physics Letters* **2004,** *396* (4-6), 393-397.

30. Marques-Gonzalez, S.; Matsushita, R.; Kiguchi, M., Surface enhanced Raman scattering of molecules in metallic nanogaps. *Journal of Optics* **2015,** *17* (11).

31. (a) Lee, Y.; Abasaki, M.; Portela, A.; Delaunay, J. J., Effective light concentration in gold short nanosphere chain on platinum mirror for surface-enhanced Raman scattering. *Applied Physics Letters* **2014,** *105* (12); (b) Lee, D.; Yoon, S., Gold Nanocube-Nanosphere Dimers: Preparation, Plasmon Coupling, and Surface-Enhanced Raman Scattering. *Journal of Physical Chemistry C* **2015,** *119* (14), 7873-7882.

32. Driskell, J. D.; Shanmukh, S.; Liu, Y. J.; Chaney, S. B.; Tang, X. J.; Zhao, Y. P.; Dluhy, R. A., The Use of Aligned Silver Nanorod Arrays Prepared by Oblique Angle Deposition as Surface-Enhanced Raman Scattering Substrates (vol 112, pg 895, 2008). *Journal of Physical Chemistry C* **2011,** *115* (40), 20052-20052.

33. Liu, X. F.; Gozubenli, N.; Choi, B.; Jiang, P.; Meagher, T.; Jiang, B., Templated fabrication of periodic arrays of metallic and silicon nanorings with complex nanostructures. *Nanotechnology* **2015,** *26* (5).

34. Etchegoin, P. G.; Le Ru, E. C., A perspective on single molecule SERS: current status and future challenges. *Physical Chemistry Chemical Physics* **2008,** *10* (40), 6079-6089.

35. Andersen, P. C.; Jacobson, M. L.; Rowlen, K. L., Flashy silver nanoparticles. *Journal of Physical Chemistry B* **2004,** *108* (7), 2148-2153.

36. Le Ru, E. C.; Meyer, M.; Etchegoin, P. G., Proof of single-mokeule sensitivity in surface enhanced Raman scattering (SERS) by means of a two-analyte technique. *Journal of Physical Chemistry B* **2006,** *110* (4), 1944-1948.

37. Domke, K. F.; Zhang, D.; Pettinger, B., Enhanced Raman spectroscopy: Single molecules or carbon? *Journal of Physical Chemistry C* **2007,** *111* (24), 8611-8616.

38. Blackie, E.; Le Ru, E. C.; Meyer, M.; Timmer, M.; Burkett, B.; Northcote, P.; Etchegoin, P. G., Bi-analyte SERS with isotopically edited dyes. *Physical Chemistry Chemical Physics* **2008,** *10* (28), 4147-4153.

39. (a) Chauhan, S. K.; Punjabi, N.; Sharma, D. K.; Mukherji, S., A silicon nitride coated LSPR based fiber-optic probe for possible continuous monitoring of sucrose content in fruit juices. *Sensors and Actuators B-Chemical* **2016,** *222*, 1240-1250; (b) Agranovich, V. M.; La Rocca, G. C., Organic-inorganic heterostructures for nonlinear optics. *Journal of Luminescence* **2016,** *169*, 422-425; (c) Dai, H. W.; Yu, Y.; Wang, X.; Ma, Z. W.; Chen, C.; Zhou, Z. K.; Han, J. B.; Han, Y. B.; Liu, S. D.; Li, L., Study of Surface Plasmon Induced Hot Electron Relaxation Process and Third-Order Optical Non linearity in Gold Nanostructures. *Journal of Physical Chemistry C* **2015,** *119* (48), 27156-27161.

40. Oberdorster, G.; Oberdorster, E.; Oberdorster, J., Nanotoxicology: An emerging discipline evolving from studies of ultrafine particles. *Environmental Health Perspectives* **2005,** *113* (7), 823-839.

41. (a) Ariga, K.; Hill, J. P.; Ji, Q. M., Layer-by-layer assembly as a versatile bottom-up nanofabrication technique for exploratory research and realistic application. *Physical Chemistry Chemical Physics* **2007,** *9* (19), 2319-2340; (b) Elechiguerra, J. L.; Reyes-Gasga, J.; Yacaman, M. J., The role of twinning in shape evolution of anisotropic noble metal nanostructures. *Journal of Materials Chemistry* **2006,** *16* (40), 3906-3919.

42. Jensen, T. R.; Malinsky, M. D.; Haynes, C. L.; Van Duyne, R. P., Nanosphere lithography: Tunable localized surface plasmon resonance spectra of silver nanoparticles. *Journal of Physical Chemistry B* **2000,** *104* (45), 10549-10556.

43. Hulteen, J. C.; Vanduyne, R. P., NANOSPHERE LITHOGRAPHY - A MATERIALS GENERAL FABRICATION PROCESS FOR PERIODIC PARTICLE

ARRAY SURFACES. *Journal of Vacuum Science & Technology a-Vacuum Surfaces and Films* **1995,** *13* (3), 1553-1558.

44. Haynes, C. L.; Van Duyne, R. P., Nanosphere lithography: A versatile nanofabrication tool for studies of size-dependent nanoparticle optics. *Journal of Physical Chemistry B* **2001,** *105* (24), 5599-5611.

45. Haynes, C. L.; Van Duyne, R. P., Plasmon-sampled surface-enhanced Raman excitation spectroscopy. *Journal of Physical Chemistry B* **2003,** *107* (30), 7426-7433.

46. Haes, A. J.; Zou, S. L.; Schatz, G. C.; Van Duyne, R. P., A nanoscale optical biosensor: The long range distance dependence of the localized surface plasmon resonance of noble metal nanoparticles. *Journal of Physical Chemistry B* **2004,** *108* (1), 109-116.

47. Hao, E.; Schatz, G. C., Electromagnetic fields around silver nanoparticles and dimers. *Journal of Chemical Physics* **2004,** *120* (1), 357-366.

48. Yamaguchi, Y.; Ishikawa, M.; Maruyama, Y.; Futamata, M., Trigonal silver nanostructure for single molecule detection with surface enhanced Raman scattering. *Journal of the Korean Physical Society* **2005,** *47*, S56-S62.

49. Zrimsek, A. B.; Henry, A. I.; Van Duyne, R. P., Single Molecule Surface-Enhanced Raman Spectroscopy without Nanogaps. *Journal of Physical Chemistry Letters* **2013,** *4* (19), 3206-3210.

50. Jensen, T. R.; Schatz, G. C.; Van Duyne, R. P., Nanosphere lithography: Surface plasmon resonance spectrum of a periodic array of silver nanoparticles by ultraviolet-visible extinction spectroscopy and electrodynamic modeling. *Journal of Physical Chemistry B* **1999,** *103* (13), 2394-2401.

51. (a) Usman, R.; Mihata, A.; Kurawaki, J., Rapid Synthesis and Characterization of Polyvinylpyrrolidone-Protected Silver Nanoparticles by Heating Method. *E-Journal of Surface Science and Nanotechnology* **2015,** *13*, 431-434; (b) Li, Z. X.; Zhao, A. W.; Gao, Q.; Guo, H. Y.; Wang, D. P.; Li, L., Fabrication of Superparamagnetic Fe3O4/Au@Ag and Its SERS Performance. *Acta Chimica Sinica* **2015,** *73* (8), 847-850; (c) Liu, C.; Chen, L.; Ren, H. H.; Zhou, J., Preparation of Nanoparticles-Modified Silica Monolith for on-Column Surface Enhanced Raman Spectroscopy. *Spectroscopy and Spectral Analysis* **2014,** *34* (5), 1289-1292.

52. Le Ru, E. C.; Grand, J.; Felidj, N.; Aubard, J.; Levi, G.; Hohenau, A.; Krenn, J. R.; Blackie, E.; Etchegoin, P. G., Experimental verification of the SERS electromagnetic model beyond the vertical bar E vertical bar(4) approximation: Polarization effects. *Journal of Physical Chemistry C* **2008,** *112* (22), 8117-8121.

53. Le Ru, E. C.; Galloway, C.; Etchegoin, P. G., On the connection between optical absorption/extinction and SERS enhancements. *Physical Chemistry Chemical Physics* **2006,** *8* (26), 3083-3087.

54. Ru, E. C.; Etchegoin, P. G.; Grand, J.; Felidj, N.; Aubard, J.; Levi, G.; Hohenau, A.; Krenn, J. R., Surface enhanced Raman spectroscopy on nanolithography-prepared substrates. *Current Applied Physics* **2008,** *8* (3-4), 467-470.

55. Haynes, C. L.; McFarland, A. D.; Zhao, L. L.; Van Duyne, R. P.; Schatz, G. C.; Gunnarsson, L.; Prikulis, J.; Kasemo, B.; Kall, M., Nanoparticle optics: The importance of radiative dipole coupling in two-dimensional nanoparticle arrays. *Journal of Physical Chemistry B* **2003,** *107* (30), 7337-7342.

56. Peyratout, C.; Donath, E.; Daehne, L., Electrostatic interactions of cationic dyes with negatively charged polyelectrolytes in aqueous solution. *Journal of Photochemistry and Photobiology a-Chemistry* **2001,** *142* (1), 51-57.

57. Hildebrandt, P.; Stockburger, M., SURFACE-ENHANCED RESONANCE RAMAN-SPECTROSCOPY OF RHODAMINE-6G ADSORBED ON COLLOIDAL SILVER. *Journal of Physical Chemistry* **1984,** *88* (24), 5935-5944.

58. Jensen, L.; Schatz, G. C., Resonance Raman scattering of rhodamine 6G as calculated using time-dependent density functional theory. *Journal of Physical Chemistry A* **2006,** *110* (18), 5973-5977.

59. McFarland, A. D.; Young, M. A.; Dieringer, J. A.; Van Duyne, R. P., Wavelength-scanned surface-enhanced Raman excitation spectroscopy. *Journal of Physical Chemistry B* **2005,** *109* (22), 11279-11285.

60. Galloway, C. M.; Le Ru, E. C.; Etchegoin, P. G., An Iterative Algorithm for Background Removal in Spectroscopy by Wavelet Transforms. *Applied Spectroscopy* **2009,** *63* (12), 1370-1376.

61. Roessner, U.; Luedemann, A.; Brust, D.; Fiehn, O.; Linke, T.; Willmitzer, L.; Fernie, A. R., Metabolic profiling allows comprehensive phenotyping of genetically or environmentally modified plant systems. *Plant Cell* **2001,** *13* (1), 11-29.

62. Seljak, U.; Slosar, A.; McDonald, P., Cosmological parameters from combining the Lyman-alpha forest with CMB, galaxy clustering and SN constraints. *Journal of Cosmology and Astroparticle Physics* **2006,** (10).

63. Karl, T. R.; Wang, W. C.; Schlesinger, M. E.; Knight, R. W.; Portman, D., A METHOD OF RELATING GENERAL-CIRCULATION MODEL SIMULATED CLIMATE TO THE OBSERVED LOCAL CLIMATE .1. SEASONAL STATISTICS. *Journal of Climate* **1990,** *3* (10), 1053-1079.

64. Jolliffe, I., *Principal Component Analysis*. Springer: Berlin, 2002.

65. dos Santos, D. P.; Andrade, G. F. S.; Temperini, M. L. A.; Brolo, A. G., Electrochemical Control of the Time-Dependent Intensity Fluctuations in Surface-Enhanced Raman Scattering (SERS). *Journal of Physical Chemistry C* **2009,** *113* (41), 17737-17744.

66. Scott, D. W., On optimal and data-based histograms. *Biometrika* **1979,** *66* (3), 605-610.

67. Kreyszig, E., Advanced Engineering Mathematics. In *J. Wiley & Sons*, J. Wiley & Sons: 1972.

68. Rodgers, J. L.; Nicewander, W. A., 13 WAYS TO LOOK AT THE CORRELATION-COEFFICIENT. *American Statistician* **1988,** *42* (1), 59-66.

69. David P. Doane, L. E. S., Measuring Skewness: A Forgotten Statistic? *Journal of Statistics Education* **2011,** *19*, 1-18.

70. Westfall, P. H., Kurtosis as Peakedness, 1905-2014. RIP. *American Statistician* **2014,** *68* (3), 191-195.

71. Lin, W. C.; Huang, S. H.; Chen, C. L.; Chen, C. C.; Tsai, D.; Chiang, H. P., Controlling SERS intensity by tuning the size and height of a silver nanoparticle array. *Applied Physics a-Materials Science & Processing* **2010,** *101* (1), 185-189.

72. Haes, A. J.; Zou, S. L.; Schatz, G. C.; Van Duyne, R. P., Nanoscale optical biosensor: Short range distance dependence of the localized surface plasmon resonance of noble metal nanoparticles. *Journal of Physical Chemistry B* **2004,** *108* (22), 6961-6968.

73. Mahmoud, M. A.; El-Sayed, M. A., Aggregation of Gold Nanoframes Reduces, Rather Than Enhances, SERS Efficiency Due to the Trade-Off of the Inter- and Intraparticle Plasmonic Fields. *Nano Letters* **2009,** *9* (8), 3025-3031.